energy&fuels

pubs.acs.org/EF Article

Novel Strategy To Analyze Fourier Transform Ion Cyclotron Resonance Mass Spectrometry Data of Biomass Pyrolysis Oil for Oligomeric Structure Assignment

Evan Terrell and Manuel Garcia-Perez*

Cite This: *Energy Fuels* 2020, 34, 8466−8481 Read Online

ACCESS | Metrics & More | Article Recommendations | Supporting Information

ABSTRACT: Among the most prominent challenges for the analysis of biomass pyrolysis products is the characterization of the abundant oligomer fraction of bio-oil. This fraction is principally made up of pyrolytic lignins and dehydrated, highly modified sugar oligomers, called humins, in liquid phase. An emerging technique for analysis of this oligomer fraction is high-resolution Fourier transform ion cyclotron resonance mass spectrometry (FT-ICR MS), which allows for accurate determination of $C_xH_yO_z$ formulas for detected oligomers. Additionally, using simple dehydration and fragmentation reaction schemes, similar formulas can be developed from cellulose-, hemicellulose-, and lignin-derived oligomers, which are primary depolymerization products. In this study, FT-ICR MS analysis is coupled with combinatoric dehydration and fragmentation modeling to match experimentally detected bio-oil oligomers with hypothetical pathways for their formation during pyrolysis. In this way, we present a novel strategy by which oligomeric structures can be proposed for bio-oils. Using this approach, it becomes possible to advance the understanding of both the molecular structures comprising the bio-oil oligomer fraction and the pathways by which these structures form during biomass pyrolysis reactions.

1. INTRODUCTION

Among all potential emerging technologies for renewable and sustainable development of energy, fuels, and chemicals, bio- and thermochemical conversion of biomass shows great promise. With respect to transitioning away from fossil fuels, in particular, petroleum, biomass valorization, if properly implemented, is perhaps the only method by which carbonaceous liquid products can be obtained with the ultimate goal of overall carbon neutrality.[1−4] Biomass itself is composed of a network of three primary polymers: cellulose, hemicellulose, and lignin.[5−8] These three constituents exist in an interconnected, multiscale structure and have both comparable and contrasting depolymerization pathways during their conversion and valorization.[4,8,9] Biomass pyrolysis is one such thermochemical conversion process, taking place in an inert atmosphere at roughly 400−600 °C, producing solid-, gas-, and liquid-phase products largely through depolymerization reactions.[10−15] Several recent studies and reviews have highlighted characterization attempts aimed at understanding biomass itself and the chemical makeup and physical properties of liquid-phase pyrolysis oil (bio-oil).[8,16−27] Although not without ongoing technological challenges, this bio-oil and the products of its upgrading are among the leading green surrogates for current petro-derived chemicals.[28−30]

One of the most significant challenges facing analytical chemists and engineers interested in liquid bio-oil characterization is the large oligomeric fraction of the oil. Bio-oil typically contains about 20−25% water, 25−30% organic volatiles (C_2−C_4 light molecules, phenolic monomers, and anhydrosugars), 30−35% water-soluble oligomers, and 15−20% water-insoluble pyrolytic lignin.[31,32] A recent review from Harman-Ware and Ferrell III suggests that the development of a reliable and standardized method for determining bio-oil molecular weight distribution is still an open problem.[33] The heavy fraction, made up of non-gas chromatography/mass spectrometry (GC/MS)-detectable compounds, has largely eluded deep and meaningful structural characterization, especially in comparison to pyrolysis-derived monomers. Two examples in which heavy structures are drawn/proposed are from Stankovikj et al. (for water-soluble pyrolytic humins)[26] and Bayerbach and Meier (for water-insoluble pyrolytic lignin).[34] These structures are shown in Figure 1. Stankovikj et al. define pyrolytic humins as (quoted here directly) "highly dehydrated oligomeric compounds derived from cellulose and hemicellulose depolymerization products".[24] Zandvoort et al. also present a complementary non-pyrolysis-derived model of humin byproduct structures that feature significant furanic content.[35]

One of the most powerful tools for probing the nature of the oligomeric fraction of bio-oil is high-resolution Fourier transform ion cyclotron resonance mass spectrometry (FT-ICR MS).[36−39] A unique chemical formula can be assigned directly from the FT-ICR MS-measured m/z (for singly charged ions, <700 Da) if ∼1 ppm mass accuracy is achieved.[38] FT-ICR MS-based "petroleomic" analysis has been successfully

Received: May 26, 2020
Revised: June 28, 2020
Published: June 29, 2020

https://dx.doi.org/10.1021/acs.energyfuels.0c01687
Energy Fuels 2020, 34, 8466−8481

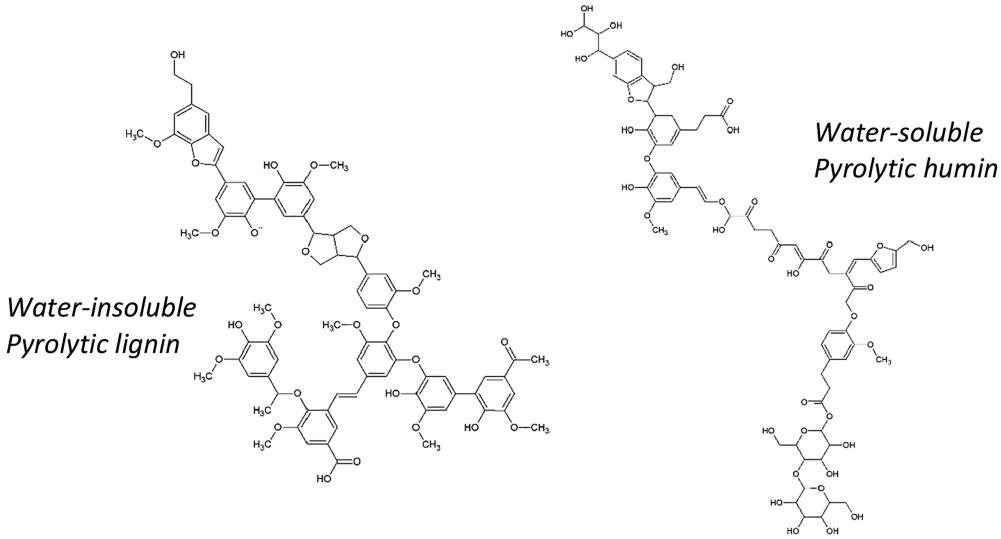

Figure 1. Representations of bio-oil oligomer molecules. This figure was adapted with permission from ref 26 (Copyright 2017 American Chemical Society; water-soluble pyrolytic humin) and ref 34 (Copyright 2009 Elsevier; water-insoluble pyrolytic lignin).

applied to the characterization of many types of materials, including petroleum,[40,41] asphaltenes,[42−44] natural/dissolved organic matter,[45−48] different biomass varieties,[16,49−53] and biomass conversion products.[22,23,54−59] Hertzog et al. present a comprehensive petroleomic analysis of bio-oil using a range of ionization techniques.[23] These authors highlight complementary differences between their characterization approaches, especially with regard to detected heteroatom class and resulting H/C and O/C ratios among assigned bio-oil oligomer chemical formulas. Olcese et al. characterized biomass pyrolysis oil and its catalytic hydrotreatment using petroleomic FT-ICR MS analysis.[60] Similarly, Ware et al. recently detailed the chemical composition of bio-oil and its hydrotreatment products using FT-ICR MS.[61] These two published studies highlight the utility of FT-ICR MS for analyzing bio-oil and its evolution in chemical nature during reactive upgrading.

Although there is a growing body of research focused on bio-oil FT-ICR MS-determined chemical formulas, at present, there is a relative paucity of available literature in which these assigned formulas are connected to literal biomass-derived molecular structures larger than monomers. Recently published work has shown that it is possible to propose candidate structures for lignin oligomers detected in FT-ICR MS (although isomer differentiation remains a challenge).[53] This work relies on coupling stochastic modeling of lignin biosynthesis and structure[62−64] with lab-based analytical chemistry measurements.[53] This type of coupling between hypothetical/theoretical computationally derived structures and experimentally observed oligomer ions is made possible by the existence of a large body of existing knowledge on the molecular structure of biomass and its pyrolysis products.[11−13,31,65−72] Once a representative set of molecular structures can be proposed and drawn, it then becomes possible to estimate properties of bio-oil molecules. Some of these properties include the boiling point, heat of vaporization, and solubility parameters, for which empirical group contribution methods exist.[31,73−76] Conjecturing the pathways by which MS-detected oligomeric products are formed can also enable progress toward more fully developed microkinetic models of biomass decomposition.

The goal of this work is to use FT-ICR MS analysis coupled with simple pyrolysis reaction network modeling to characterize more fully the heavy fraction of pyrolysis oil, thereby allowing for the proposal of candidate structures to abundant bio-oil compounds. This can then be used as a basis for understanding dehydration and fragmentation pathways that may govern biomass pyrolysis reactions in the liquid intermediate.

2. METHODOLOGY

2.1. Biomass Pyrolysis and Bio-oil Characterization. The data for FT-ICR MS analysis used here is derived from previous work by Stankovikj et al.[24] The bio-oil samples in this work are from a commercial rotating cone reactor (BTG) and fluidized bed operated at a low temperature (15A) and a high temperature (22A) (naming convention adopted from the initial Stankovikj et al. study). All oils are produced from pine wood. The BTG oil was produced at an average reactor temperature of 510 °C and average wood particle size of 3 mm. The 15A and 22A oils were produced at fluidized bed temperatures of 330 and 580 °C, respectively, and an average wood particle size of 1 mm. In both reactor types (i.e., fluidized bed and rotating cone), bio-oil is collected similarly from cooling and condensation of hot vapor-phase products leaving the reactor. Char is separated with cyclones. The primary difference between reactors is the presence of inert gas for heat transfer in a fluidized bed, while a rotating cone relies only on mechanical mixing between biomass and inert sand. A figure with pyrolysis reactor schematics is given in the Supporting Information.[77] Further details on these oils and their production are available in previous work.[24,77−79]

The bio-oils in the Stankovikj et al. study are characterized with the following techniques: water content, GC/MS, hydrolyzable sugars, total carbohydrates, pyrolytic lignin quantification, elemental analysis, FT-ICR MS, functional group titrations, weak acid and phenol titration, total phenols, ^{31}P nuclear magnetic resonance (NMR), ^{1}H NMR, attenuated total reflection (ATR)−Fourier transform infrared spectroscopy (FTIR), and ultraviolet (UV) fluorescence.[24] Specifically of interest in this work are elemental analysis, GC/MS, and FT-ICR MS.

Elemental analysis was performed using a Leco TruSpec CHN 628 instrument following the ASTM D5373-08 standard method, with the oxygen content determined by difference.[24] GC/MS was performed using Agilent Technologies 7890A GC with a Restek Rtx-1701 column (60 m × 250 μm × 0.28 μm) and Agilent 5975 C MS. Bio-oil samples were dissolved in acetonitrile for GC/MS analysis at 10% oil

https://dx.doi.org/10.1021/acs.energyfuels.0c01687
Energy Fuels 2020, 34, 8466−8481

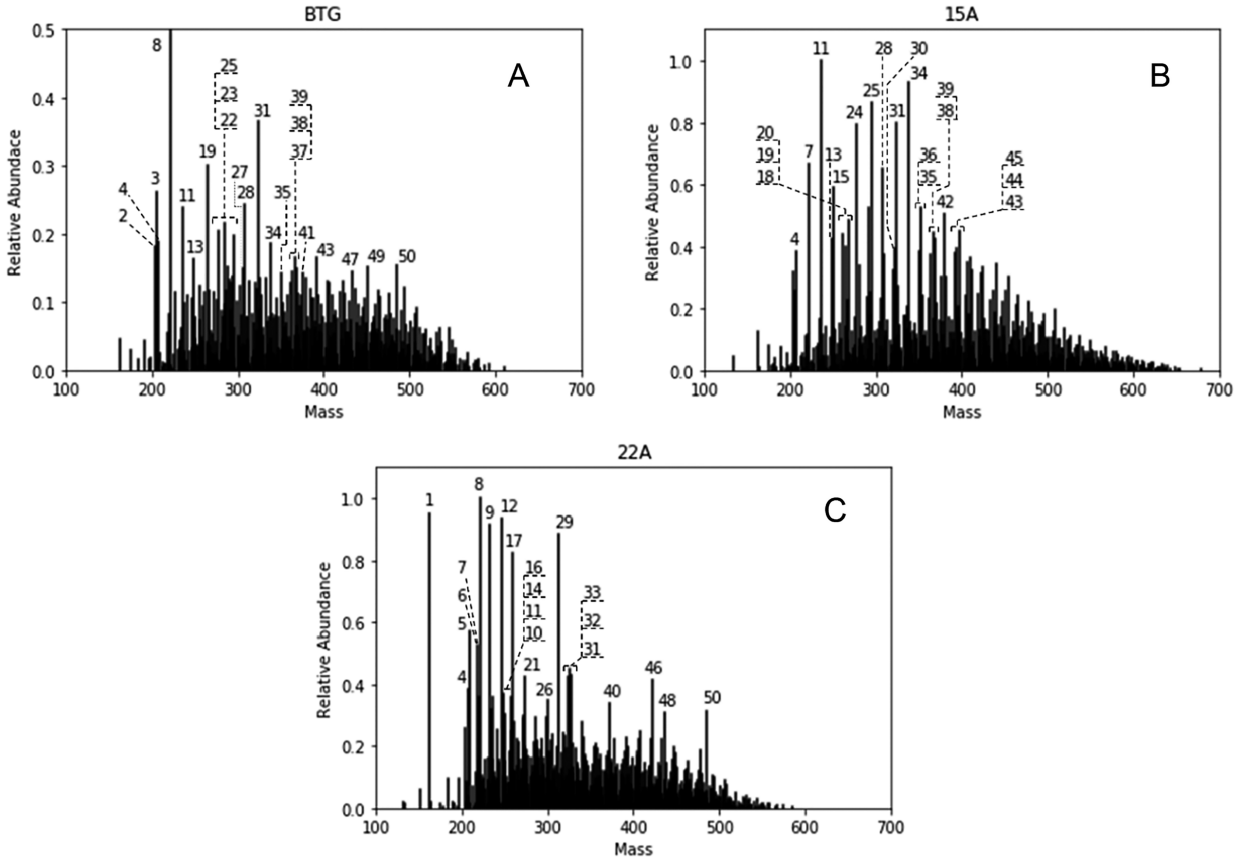

Figure 2. Representations of the FT-ICR mass spectra for (A) BTG, (B) 15A, and (C) 22A bio-oils (numbered peaks correspond to the proposed pathways/structures in Table 4). The vertical axis of BTG is rescaled to a maximum of 0.5, with peak number 8 extending to an abundance value of 1.0.

concentration. Isoamyl ether, 1-octanol, and methyl laurate were used as internal standards, and eight-point calibration curves were built for 34 standard compounds for quantification.[24] FT-ICR MS analysis was performed on the bio-oils in negative ion mode using electrospray ionization (ESI) with a Bruker Solarix 9.4T instrument. Bio-oil samples were diluted 10 mg/mL in methanol for analysis. The FT-ICR MS result peak list was produced by Bruker DataAnalysis and assessed for formula assignment with Composer software (Sierra Analytics). Mass accuracy was limited to 3 ppm, and relative ion abundance was limited to 0.1%. A more complete, detailed description of all bio-oil characterization performed by Stankovikj et al. is available in their original publication.[24]

2.2. Combinatoric Depolymerization−Dehydration−Fragmentation Pyrolysis Model. This model is based on a simplified interpretation of reacting biomass presented by Marathe et al.[80] (see Figure S2 of the Supporting Information), with the consideration of limited, specific reactive fragmentations. Each constituent polymer (i.e., cellulose, hemicellulose, and lignin) was treated separately. Our analysis supposes that the biomass constituents are first depolymerized into oligomers (2−4 monomeric units) with a boiling point close to those allowing for removal by evaporation. Heavier oligomers formed (more than 4 monomeric units) are also subjected to dehydration and fragmentation, but the achievable reductions in molecular weight are not sufficient to allow for their removal by evaporation. These heavy oligomers are the main intermediate precursors for solid-phase char production.[71,72] In our analysis, we include only the small oligomers, because the heavy oligomers are not likely to result in liquid-phase molecules within the molecular weight range measured by FT-ICR MS. On the basis of hypothetical dehydration and fragmentation pathways, a simple combinatoric model of potential pyrolysis products was built up from biomass depolymerization intermediates. The model of cellulose pyrolysis begins from hexose-based polymer fragments with a degree of polymerization (d_p) of up to 4 and considers dehydration, decarbonylation, and the loss of $C_3H_6O_2$ (for acetol) and $C_2H_4O_2$ (for glycolaldehyde). These reactions lead to the formation of the most important fragmentation products reported during cellulose pyrolysis.[11,81] The model of hemicellulose pyrolysis begins from all possible combinations of hexose and pentose polymer fragments up to d_p = 4 and considers dehydration and decarbonylation. The model of lignin pyrolysis begins from guaiacyl β−O−4 polymer fragments (as a result of the nearly 100% guaiacyl makeup of softwood pine lignin[82]) of up to d_p = 3 and considers dehydration, dehydroxylation, and demethylation. Fragmentations of phenyl glucosides (d_p = 2,3) are also lumped in with the lignin model (for the lignin−carbohydrate complex) and include dehydration, decarbonylation, dehydroxylation, and demethylation. A descriptive set of figures of the combinatorics underlying the fragmentation modeling is given in the Supporting Information. Data manipulation and visualization are performed with Microsoft Excel and Python.

3. RESULTS AND DISCUSSION

3.1. Analysis of Experimental Bio-oil FT-ICR MS. Representations of the mass spectra for the bio-oils analyzed in this study (BTG, 15A, and 22A) are given in Figure 2. As in previous biomass FT-ICR MS work on lignin, for relevant figures throughout this work, the term "mass" is used on the x axis; this refers to the nominal mass calculated for each assigned formula (such that C = 12, H = 1, and O = 16) from each respective m/z value detected during MS analysis.[53]

The detected peaks have mass within the range of approximately 150−650 Da. The carbon number and oxygen number breakdown with respect to relative abundance is given in Figure 3. The most abundant carbon and oxygen numbers

https://dx.doi.org/10.1021/acs.energyfuels.0c01687
Energy Fuels 2020, 34, 8466−8481

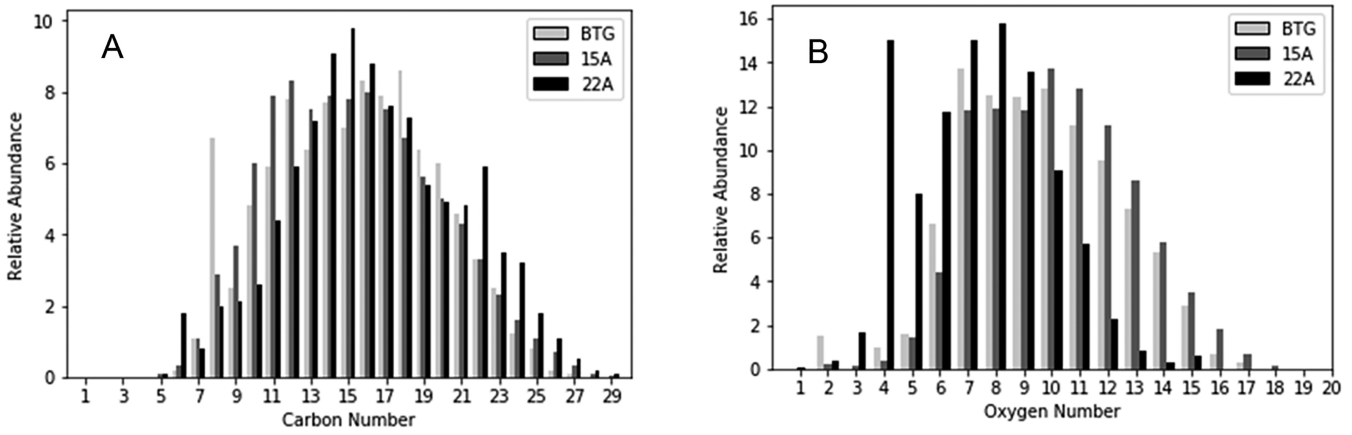

Figure 3. Detected bio-oil oligomer (A) carbon number and (B) oxygen number plotted against the relative MS abundance.

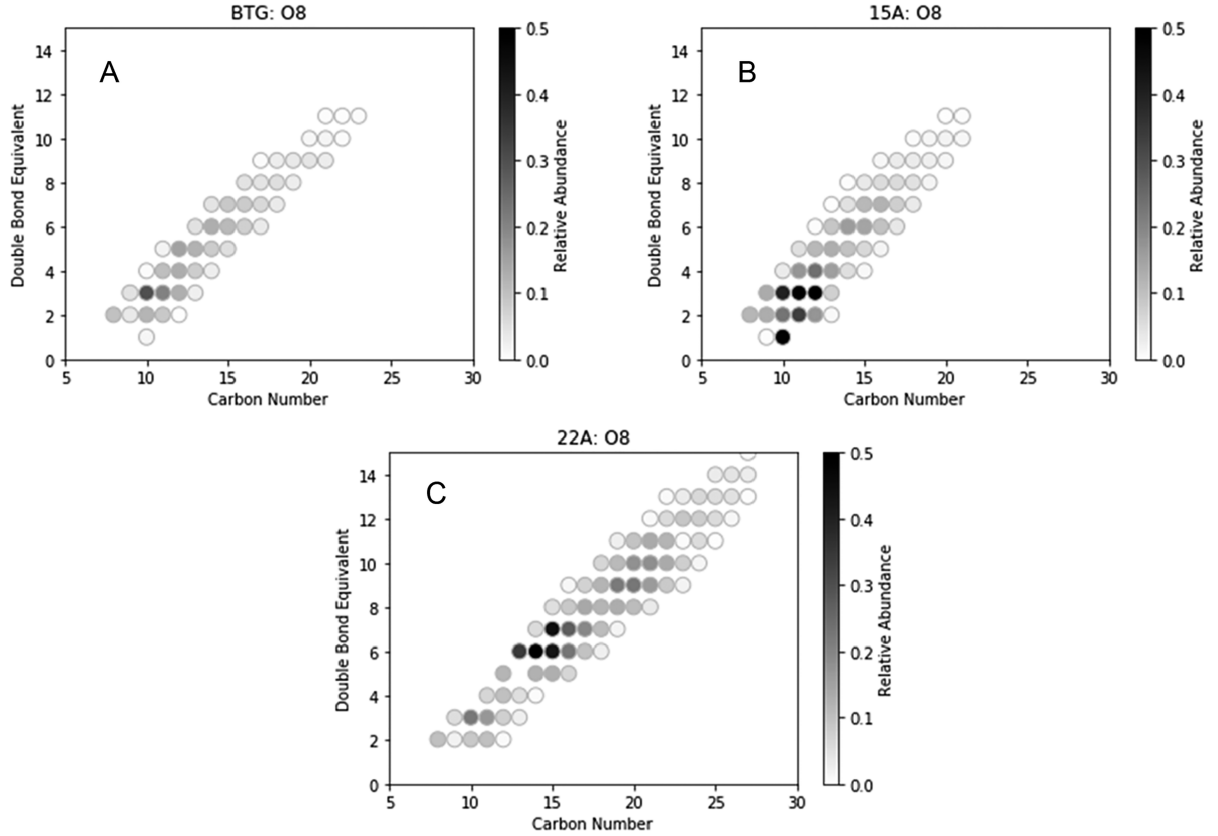

Figure 4. Carbon number versus DBE for (A) BTG, (B) 15A, and (C) 22A bio-oils of oxygen class O8 (with relative MS abundance on grayscale color bar; all points with abundance of >0.5 are black).

are between roughly 13−17 and 7−11, respectively. These values correspond well with what could be expected from biomass-derived dimers and trimers from holocellulose (i.e., cellulose and hemicellulose) and lignin. The 22A bio-oil, in comparison to the other two samples, tends to have greater abundance for higher carbon numbers and lower oxygen numbers. This may be attributed to its higher content of pyrolytic lignin and/or humins.[24] Figure 4 depicts the double bond equivalent (DBE) versus carbon number for one abundant oxygen class (O8) from each bio-oil. The presence of monotonically increasing DBE with increasing carbon number suggests that the detected MS peaks are from linear oxygenated oligomers (in contrast with a more complex bimodal distribution that is characteristic of samples with a more significant hydrocarbon content).[61,83]

Two other data visualization modes with great utility for assessing FT-ICR MS data are the van Krevelen diagram[84,85] and the carbon versus mass diagram.[86] van Krevelen diagrams for the studied bio-oils are given in Figure 5. The O/C ratio values range from approximately 0.2 to 1.0, and the H/C ratio values range from approximately 0.6 to 2.0. These values are appropriately consistent with the ranges of O/C and H/C that are expected for lignin- and holocellulose-derived compounds.[48,84] The BTG and 15A samples show greater abundance in the cellulose region (O/C ≈ 0.7−1.0; H/C ≈ 1.5−2.0). The 22A sample, unlike BTG and 15A, also has high-

https://dx.doi.org/10.1021/acs.energyfuels.0c01687
Energy Fuels 2020, 34, 8466−8481

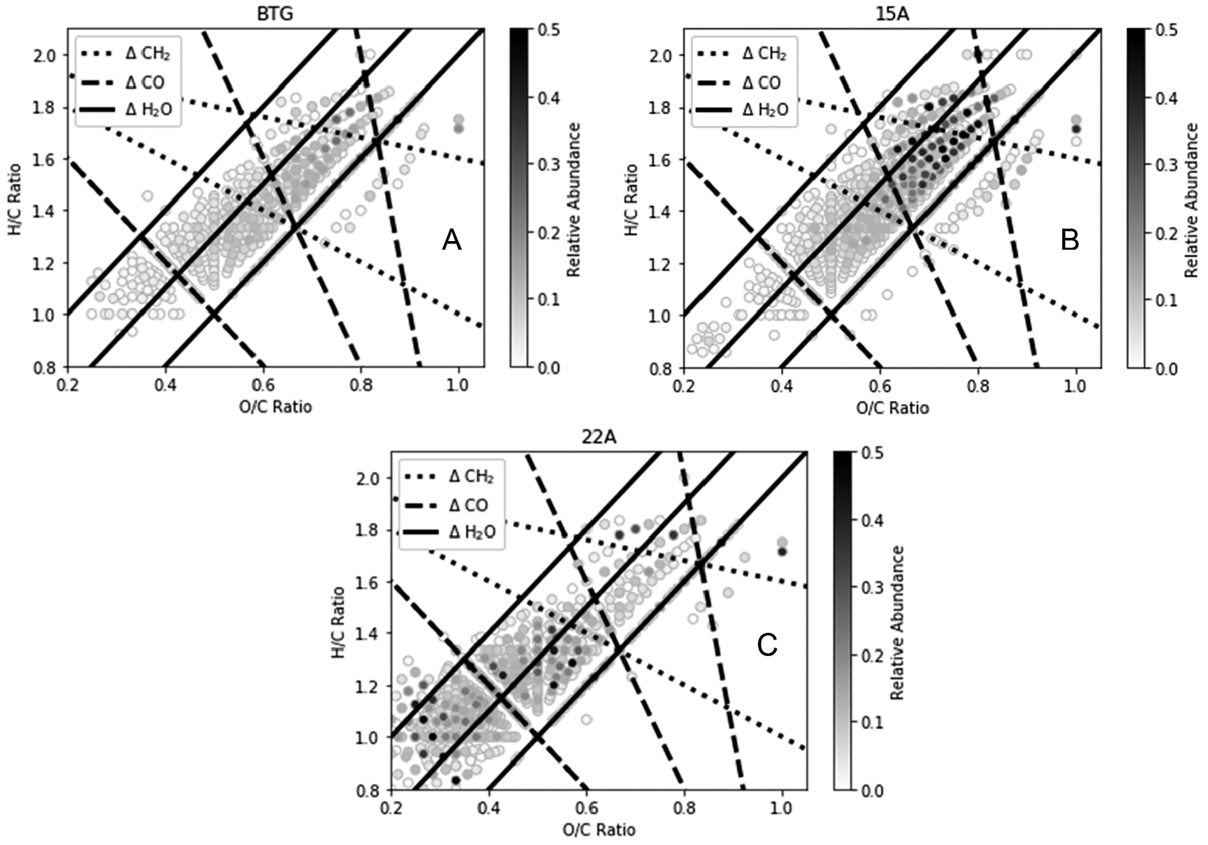

Figure 5. van Krevelen diagrams with lines representing changes in methyl, carbonyl, and water to $C_xH_yO_z$ formulas for (A) BTG, (B) 15A, and (C) 22A bio-oils (with relative MS abundance on grayscale color bar; all points with abundance of >0.5 are black).

Table 1. Algebraic Expressions Describing the Linear Characteristics on van Krevelen Diagrams

group	initial assumption	slope (m)	vertical intercept (b)	horizontal intercept ($-b/m$)
$C_xH_yO_z$	$C_p = C_q - xn$ $H_p = H_q - yn$ $O_p = O_q - zn$	$(x\mathrm{H} - y\mathrm{C})/(x\mathrm{O} - z\mathrm{C})$	$\mathrm{H/C} - \mathrm{O}(x\mathrm{H} - y\mathrm{C})/\mathrm{C}(x\mathrm{O} - z\mathrm{C})$	$\mathrm{O/C} - \mathrm{H}(x\mathrm{O} - z\mathrm{C})/\mathrm{C}(x\mathrm{H} - y\mathrm{C})$
H_yO_z	$C_p = C_q$ $H_p = H_q - yn$ $O_p = O_q - zn$	y/z	$(z\mathrm{H} - y\mathrm{O})/z\mathrm{C}$	$(y\mathrm{O} - z\mathrm{H})/y\mathrm{C}$
C_xH_y	$C_p = C_q - xn$ $H_p = H_q - yn$ $O_p = O_q$	$(x\mathrm{H} - y\mathrm{C})/x\mathrm{O}$	y/x	$y\mathrm{O}/(y\mathrm{C} - x\mathrm{H})$
C_xO_z	$C_p = C_q - xn$ $H_p = H_q$ $O_p = O_q - zn$	$x\mathrm{H}/(x\mathrm{O} - z\mathrm{C})$	$z\mathrm{H}/(z\mathrm{C} - x\mathrm{O})$	z/x

abundance points in the lignin/humin region of the van Krevelen diagram (O/C ≈ 0.2−0.5; H/C ≈ 0.8−1.3)[35,53] as a result of its greater abundance of pyrolytic lignin and/or humins.

On the basis of the presence of some linear patterns in a van Krevelen diagram, it is possible to deduce some potential regular changes in functional groups or chemical reactions, as suggested by Kim et al.[84] These characteristic lines can be further algebraically assessed, as shown in eqs 1 and 2. Equation 1 describes the slope (m) between two arbitrary points (p and q), and eq 2 describes the characteristic line in slope−intercept form ($b = y$ intercept). This type of approach is briefly presented in early work from Tang and Bacon and more recently in work from Wu et al. regarding van Krevelen diagram analysis.[85,87] The resulting algebraic governing expressions for characteristic van Krevelen lines are given in Table 1.

$$m = \frac{\Delta\left(\frac{\mathrm{H}}{\mathrm{C}}\right)}{\Delta\left(\frac{\mathrm{O}}{\mathrm{C}}\right)} = \frac{\mathrm{C}_q\mathrm{H}_p - \mathrm{C}_p\mathrm{H}_q}{\mathrm{C}_q\mathrm{O} - \mathrm{C}_p\mathrm{O}_q} \quad (1)$$

$$\frac{\mathrm{H}}{\mathrm{C}} = m\frac{\mathrm{O}}{\mathrm{C}} + b \quad (2)$$

Regardless of the starting point on a van Krevelen diagram, a change in the molecular formula involving only two atomic species (e.g., CO, CO_2, H_2O, and CH_2) will produce a line with either a constant intercept or a constant slope. These invariant characteristics are illustrated in Table 1. This result does not necessarily imply the inverse: that the existence of an

https://dx.doi.org/10.1021/acs.energyfuels.0c01687
Energy Fuels 2020, 34, 8466−8481

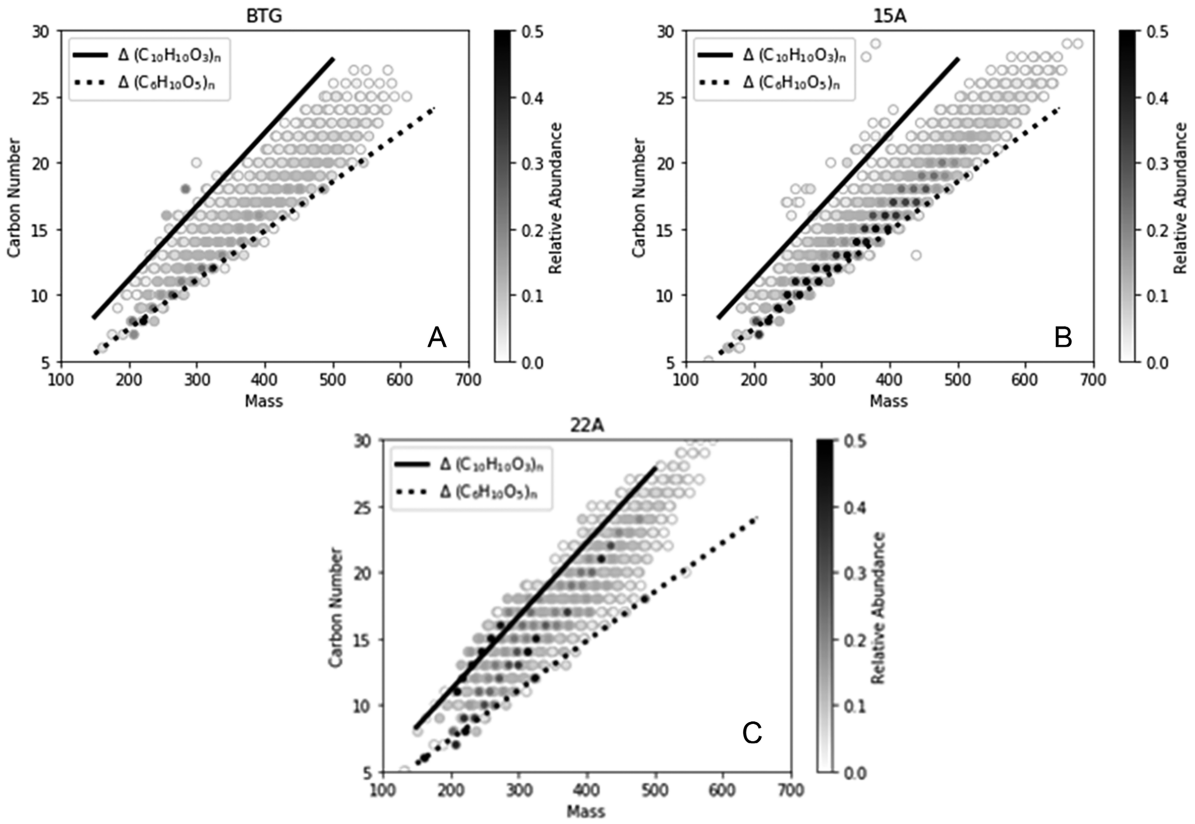

Figure 6. Carbon number versus mass, with lines representing changes of hypothetical lignin (solid line) and holocellulose (dotted line) for (A) BTG, (B) 15A, and (C) 22A bio-oils (with relative MS abundance on grayscale color bar; all abundances of >0.5 are black).

individual line with a certain slope or intercept corresponds to some constant change in the formula. For example, removing methanol from cellobiose (from $C_{12}H_{22}O_{11}$ to $C_{11}H_{20}O_{10}$) produces a line with a slope of 2, y intercept of 0, and x intercept of 0. However, removing a methanol from dehydoxylated cellobiosan (from $C_{12}H_{20}O_9$ to $C_{11}H_{18}O_8$) produces a line with a slope of 1.33, y intercept of 0.67, and x intercept of −0.50. In this instance, the removal of methanol from different starting points yields different slopes and intercepts. Conversely, dehydration of cellobiose (from $C_{12}H_{20}O_9$ to $C_{12}H_{18}O_8$) produces a slope of 2, y intercept of 0, and x intercept of 0. Dehydration of dehydroxylated cellobiosan (from $C_{12}H_{20}O_9$ to $C_{12}H_{18}O_8$) produces a slope of 2, y intercept of 0.17, and x intercept of −0.08. Although the intercept values differ, the slope is invariant for dehydration because it involves a change in only two atomic species: H and O in H_2O. Dehydration implies the existence on a van Krevelen diagram of a line with slope 2; a line with slope 2 does not necessarily imply the existence of dehydration. Analogous statements can be made for other groups of only two atomic species (e.g., CO and CH_2). Formula changes involving three atomic species do not produce invariants in slope or intercept values alone, as per the derived expressions in Table 1.

The carbon versus mass diagram for each studied bio-oil is given in Figure 6. As with the van Krevelen diagrams, the BTG and 15A samples show greater abundance in the holocellulose region at the lower/bottom end of the C versus mass plot. The 22A sample shows additional abundant peaks in the lignin/humin region; for a given mass, lignin-derived and other highly degraded compounds have a greater number of carbon atoms than that of typical holocellulose-derived compounds, which may be more oxygenated. Although the mass range extends up to approximately 650 Da, the most abundant peaks are in the 200−400 Da range. This suggests that dimers and trimers are the primary constituents of the detected compounds in the analyzed bio-oils.

The straight-line segments shown on the plots in Figure 6 correspond to hypothetical lignin and holocellulose polymers. The upper (solid) line is produced by starting at coniferyl alcohol ($C_{10}H_{12}O_3$) and proceeding by a slope resulting from regular additions of $C_{10}H_{10}O_3$ to represent hypothetical lignin. The lower (dotted) line is produced by starting at levoglucosan ($C_6H_{10}O_5$) and proceeding by a slope resulting from regular additions of $C_6H_{10}O_5$ to represent hypothetical holocellulose. The range of detected points is roughly bound by these two lines. The 22A sample extends slightly beyond the upper bound (solid line) defined by hypothetical lignin. This may be attributed to additional fragmentation reactions occurring on underlying primary pyrolysis structures, resulting from higher temperature pyrolysis reactions. Taken together, the results presented in Figures 5 and 6 indicate that FT-ICR MS-detected compounds fall within a molecular space containing primary biomass constituent oligomers (i.e., from holocellulose and lignin) and their fragmentation products, in which dehydration and decarbonylation (among other possible reactions) may be predominant.

Finally, further quantitative evaluation of the MS data also allows for the calculation of elemental analysis results for the studied bio-oils. Each bio-oil was analyzed with both GC/MS and FT-ICR MS.[24] This approach assumes that GC/MS detects only low-molecular-weight compounds (i.e., volatile

https://dx.doi.org/10.1021/acs.energyfuels.0c01687
Energy Fuels 2020, 34, 8466−8481

organics and monomers), that FT-ICR MS detects only high-molecular-weight compounds (i.e., non-volatile oligomers), and that the sum of the GC/MS and FT-ICR MS fractions is 100%. In this way, C, H, and O (%) for both the GC/MS and FT-ICR MS fractions can be calculated separately, weighted by relative MS abundance. While it is certainly possible for overlaps in detected molecular weight ranges to exist between GC/MS and FT-ICR MS, we postulate that this effect is negligible (at least regarding the MS data used here). For example, the heaviest GC/MS-detected bio-oil compounds have a molecular weight up to approximately 200 Da;[24] however, the FT-ICR MS abundance of compounds with a weight less than 200 Da is very small (Figure 2). The final elemental analysis result is then the weighted average of the GC/MS and FT-ICR MS fractions (eq 3, where n = C/H/O mass %, φ = GC/MS fraction, X = GC/MS C/H/O mass %, and Y = FT-ICR MS C/H/O mass %).

$$n = (\varphi)X + (1 - \varphi)Y \quad (3)$$

The results of the elemental analysis calculations are given in Table 2. The nitrogen content is not considered (viz., it is assumed to be negligible). The GC/MS-detected mass fractions for BTG, 15A, and 22A are 29.4, 36.7, and 37.0%, respectively.[24] There is good agreement between the elemental analysis results using GC/MS and FT-ICR MS data, as in eq 3, and the reported results from Stankovikj et al.[24] In each case, the relative difference between the calculated and reported values is within 5%. The 22A sample again shows higher carbon and lower oxygen contents, in correspondence with the results presented in previous figures. Ultimately, the elemental analysis presented here suggests that the MS-based results for the studied bio-oils comprise an accurate and reliable elemental representation of the bio-oil samples, which agrees well with other experimental characterization techniques.

Table 2. Elemental Analysis of BTG, 15A, and 22A Bio-oils Using a MS-Based Approach

	GC/MS value;[a] FT-ICR MS value			combined value (eq 3); *reported value (Stankovikj et al.)*[24]		
sample	C (%)	H (%)	O (%)	C (%)	H (%)	O (%)
BTG	49.9	7.0	43.2	50.7	6.5	42.8
	51.0	6.3	42.7	*52.6*	*6.2*	*41.1*
15A	48.6	7.1	44.3	49.2	6.6	44.2
	49.5	6.3	44.2	*50.5*	*6.5*	*43.1*
22A	47.7	7.0	45.3	54.5	6.4	39.1
	58.5	6.0	35.5	*54.1*	*6.7*	*39.2*

[a]GC/MS-detected mass fractions: BTG = 29.4%; 15A = 36.7%; and 22A = 37.0%.

3.2. Pyrolysis Model of Primary Biomass Constituents: Cellulose, Hemicellulose, and Lignin. To more fully characterize the FT-ICR MS results from a given biomass pyrolysis liquid sample, it is possible to attempt to propose specific structures that correspond to unique detected $C_xH_yO_z$ peaks. It is therefore constructive to assess what kinds of results may arise from the consideration of hypothetical depolymerization, dehydration, and/or fragmentation reactions occurring during pyrolysis of cellulose, hemicellulose, and lignin. This allows for the development of a library of $C_xH_yO_z$ formulas with known hypothetical structures, which can then be matched to observed experimental MS data. Collard and Blin report that the three main classes of primary mechanisms involved in biomass pyrolysis are char formation (not particularly relevant for liquid product analysis), depolymerization, and fragmentation.[67] Further, there is some consensus that, among primary fragmentation reactions, holocellulose dehydration is prominent, especially at lower temperatures.[11,14,65,67−70,81]

Illustrations of some initial fragmentation products (specifically from dehydration) that may occur during early biomass pyrolysis reactions are given in Figures 7, 8, and 9 for cellulose, hemicellulose, and lignin, respectively. Completely accurate stereochemistry and stoichiometry are not considered. These depictions are adapted from the cited literature for each figure and are not meant to be a rigorous overview of pyrolysis reactions occurring among biomass constituents. Further reading on the pyrolysis of cellulose,[88−90] hemicellulose,[12,65,91] and lignin[13,92,93] is available (among a myriad of potential other sources).

The combinatoric fragmentation pyrolysis model (described in section 2.2) produces a set of approximately 1200 chemical formulas, although not all are necessarily unique. The effect of

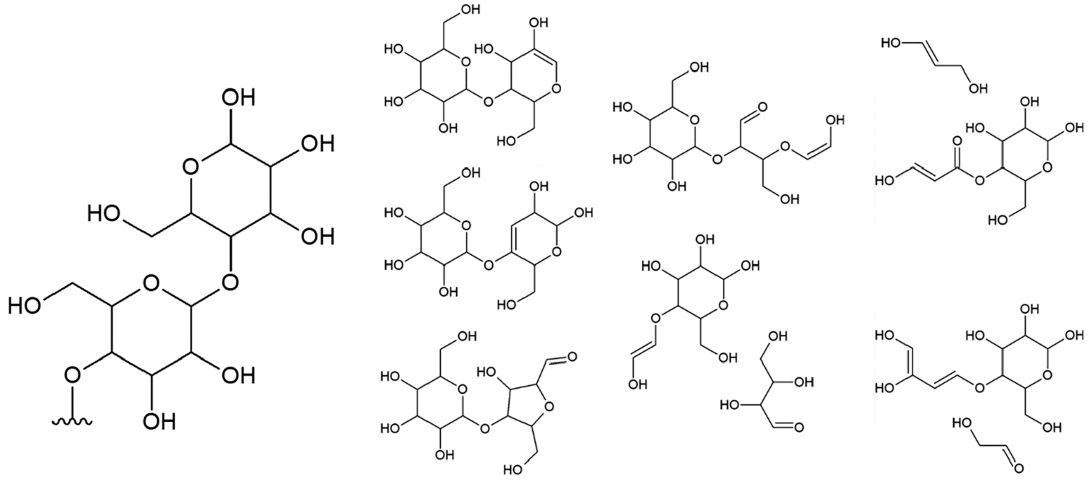

Figure 7. Representation of fragmentation products of cellulose, using the hexose model structure as the surrogate. This figure was adapted with permission from ref 81. Copyright 2018 American Chemical Society.

https://dx.doi.org/10.1021/acs.energyfuels.0c01687
Energy Fuels 2020, 34, 8466−8481

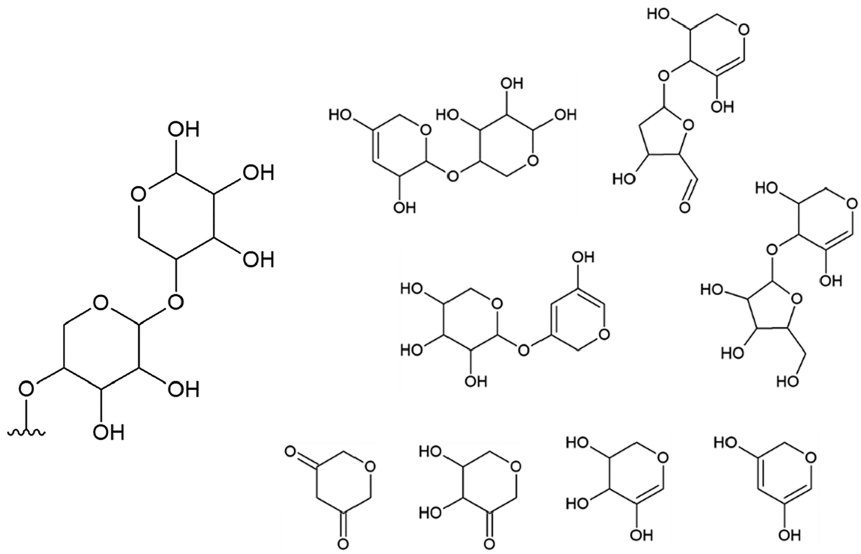

Figure 8. Representations of fragmentation products of hemicellulose, using the pentose model structure as the surrogate. This figure was adapted with permission from ref 12. Copyright 2018 Royal Society of Chemistry.

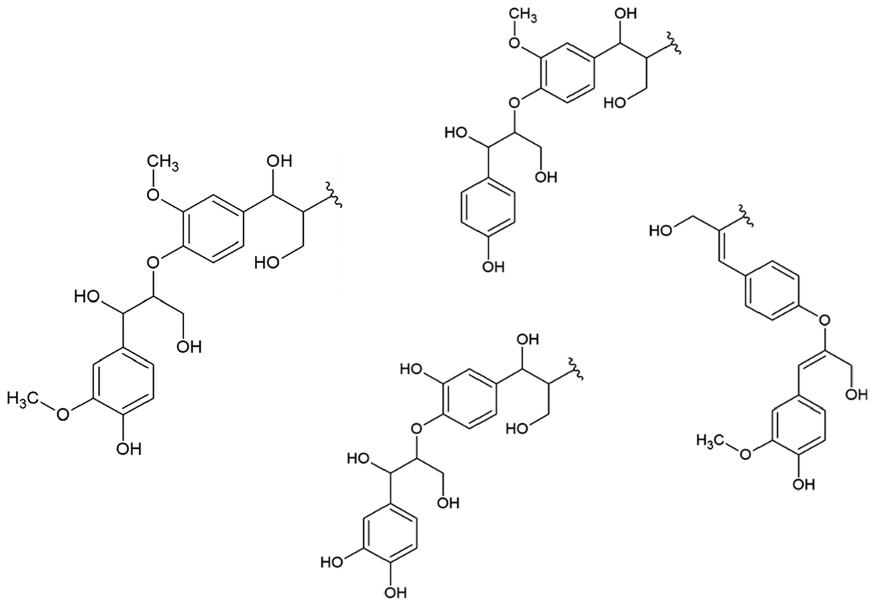

Figure 9. Representations of fragmentation products of lignin, using the guaiacyl model structure as the surrogate. This figure was adapted with permission from ref 13. Copyright 2018 American Chemical Society.

fragmentations is reflected in resulting $C_xH_yO_z$ formulas only, and no consideration is given to whether or not these formulas produce possible or realistic molecular structures; however, the presence of "unrealistic" formulas does not limit the ability of the model results to be used as a library for oligomer structure/pathway assignment. Using this combinatoric fragmentation product formula library, van Krevelen diagrams and carbon versus mass diagrams are developed, as shown Figure 10, to mirror the results shown previously in Figures 5 and 6. Figure 10 also includes experimental BTG points, for visual comparison.

In general, the results from combinatoric fragmentation modeling and experimentally observed FT-ICR MS (shown here for BTG bio-oil) correspond well, qualitatively. The cellulose and hemicellulose model points cover nearly the entire range of the experimental points on both van Krevelen and carbon versus mass diagrams. The lignin model covers the appropriate mass range (i.e., ~150−650) in identifiable clusters as a result of its nature as an aromatic polymer.[53] Because of distinctions in molecular characteristics between lignin and holocellulose (and their fragmentation products), the lignin model data exist in more discretized groups with respect to the set of points belonging to whole bio-oil shown in Figure 10. This is expected for lignin-derived compounds, which preserve their aromaticity and tend to have more carbon and less oxygen, in comparison to holocellulose, for a given molecular weight. On the van Krevelen diagram, lignin is confined to approximately O/C = 0.2−0.5 and H/C = 0.8−1.3. The uncovered experimental points for cellulose and hemicellulose at high mass could be the result of fragmentation products with d_p = 5, although their relative MS abundance is low (as in Figure 6). The combinatoric fragmentation model formulas did not consider d_p larger than 4.

https://dx.doi.org/10.1021/acs.energyfuels.0c01687
Energy Fuels 2020, 34, 8466−8481

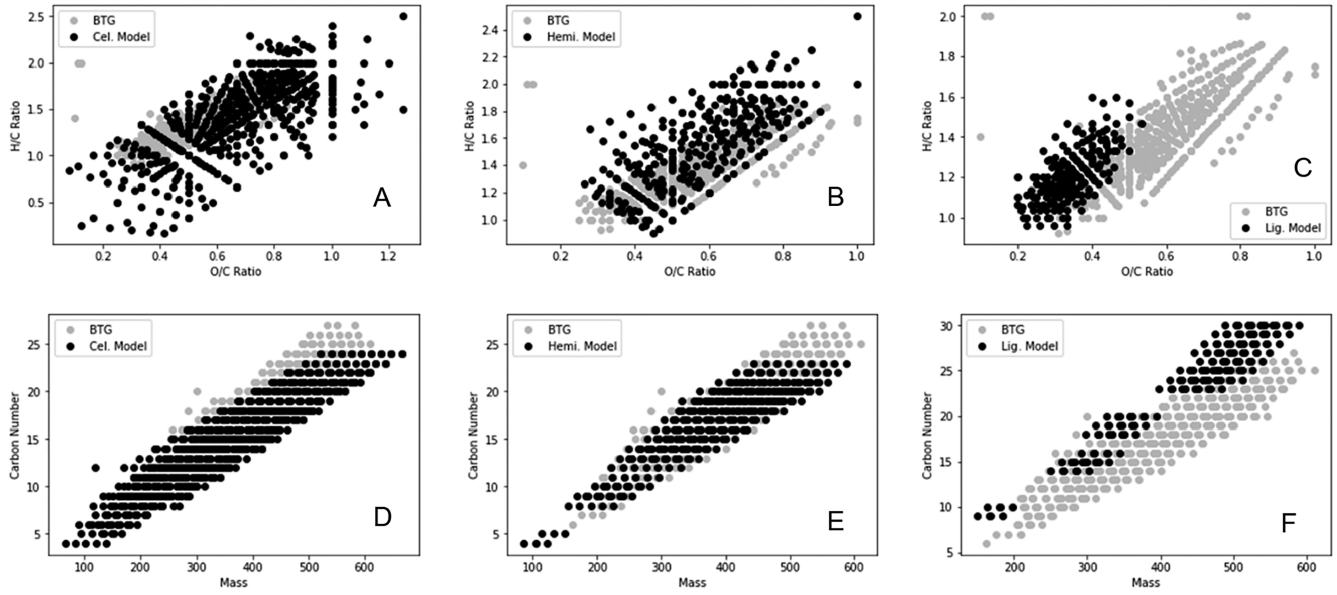

Figure 10. Representation of modeled fragmentation results showing van Krevelen diagrams for model (A) cellulose, (B) hemicellulose, and (C) lignin and C versus mass diagrams for model (D) cellulose, (E) hemicellulose, and (F) lignin. FT-ICR MS-measured results for BTG bio-oil are shown for comparison.

Table 3. Quantifiable Parameters[a] for Modeled Components and Measured Bio-oils

parameter	cellulose model	hemicellulose model	lignin model	combined model	BTG	15A	22A
C	15	17	23	17	17	18	18
	(5)	(4)	(5)	(6)	(5)	(5)	(5)
H	21	26	28	23	24	25	22
	(9)	(8)	(6)	(9)	(6)	(8)	(6)
O	10	10	8	9	10	11	8
	(4)	(3)	(2)	(4)	(3)	(4)	(3)
O/C	0.7	0.6	0.3	0.6	0.6	0.6	0.5
	(0.2)	(0.2)	(0.1)	(0.2)	(0.2)	(0.2)	(0.2)
H/C	1.4	1.5	1.2	1.4	1.4	1.4	1.3
	(0.4)	(0.3)	(0.1)	(0.4)	(0.2)	(0.3)	(0.2)
DBE	5.2	4.9	10.2	5.9	6.3	6.5	8.1
	(2.8)	(2.7)	(3.0)	(3.4)	(2.5)	(2.9)	(3.2)
MW	352	382	435	372	389	411	372
	(124)	(99)	(99)	(118)	(101)	(117)	(95)

[a]Average values for specified parameters with unweighted standard deviations in parentheses.

Finally, to quantitatively compare modeled results to experimental results, the averages and standard deviations of specific parameters were calculated. This is detailed in Table 3. Each individual model (i.e., cellulose, hemicellulose, and lignin) is shown separately and as a combined model into one larger library of formulas. Values from BTG, 15A, and 22A experimental results are also given. Relative MS abundance was not considered in calculating average and standard deviation values; i.e., each point was assumed to have equal contribution. The largest differences between the combined model and experiment in O/C, H/C, and DBE are with 22A, likely as a result of its higher pyrolytic lignin and/or humin content. For molecular weight, the largest difference is ∼40 Da for 15A, although all standard deviations are ∼100−120. The C, H, and O numbers are within 2 for all samples. Ultimately, these presented quantitative values suggest that the modeled results comprise an accurate starting point from which potential molecular structures can be matched to observed experimental bio-oil data.

3.3. Proposed Structure Assignment to Top Peaks from Bio-oil FT-ICR MS.

3.3.1. Cellulose-Derived Structures. Using the results of the combinatoric fragmentation model, potential structures are proposed for detected FT-ICR MS peaks with high abundance. Specifically, the top 23 peak formulas from each sample (BTG, 15A, and 22A) are matched to a proposed cellulose-derived structure. Because some samples share common peaks, the collection of the top 23 from each sample constitutes 50 unique structures. These results are detailed in Table 4. A hexose monomer unit is denoted as H and repeated in brackets to signify the degree of polymerization. For example, a hexose trimer (e.g., cellotriose) is given as "[HHH]". The specified fragmentations are then applied to this structure to arrive at the appropriate $C_xH_yO_z$ formula. Possible pathways (for numbers 8, 11, 12, and 34 in Table 4) are shown in Figure 11. These routes and their final structures are meant to be illustrative only, and no conformational analysis was considered for the structures themselves.

https://dx.doi.org/10.1021/acs.energyfuels.0c01687
Energy Fuels 2020, 34, 8466−8481

Table 4. Proposed Fragmentation Pathways and Resulting Structure Representation for Cellulose Oligomer-Derived Peaks among the Studied Bio-oils

number	C	H	O	mass	proposed structure	sample ID[a]
1	6	10	5	162	[H]−H_2O (levoglucosan)	22A-2
2	8	12	6	204	[HH]−2H_2O−$C_3H_6O_2$−CO	BTG-11
3	8	14	6	206	[HH]−H_2O−$C_3H_6O_2$−CO−OH	BTG-4
4	7	12	7	208	[HH]−H_2O−$C_3H_6O_2$−CO−CH_3	BTG-9, 15A-22, and 22A-14
5	11	14	4	210	[HHH]−3H_2O−2$C_3H_6O_2$−CO−4OH	22A-7
6	12	10	4	218	[HHH]−6H_2O−$C_3H_6O_2$−CO−3OH−CH_3−CH_2 (with ring contraction)	22A-8
7	9	16	6	220	[HH]−H_2O−$C_2H_4O_2$−CO−OH	22A-17
8	8	14	7	222	[HH]−H_2O−$C_3H_6O_2$−CO	BTG-1, 15A-6, and 22A-1
9	13	12	4	232	[HHH]−6H_2O−$C_3H_6O_2$−CO−3OH−CH_3	22A-4
10	13	14	4	234	[HHH]−5H_2O−$C_3H_6O_2$−CO−4OH−CH_3	22A-21
11	9	16	7	236	[HH]−H_2O−$C_2H_4O_2$−CO	BTG-6, 15A-1, and 22A-18
12	14	14	4	246	[HHH]−5H_2O−$C_2H_4O_2$−5OH−2CH_3	22A-3
13	10	16	7	248	[HH]−H_2O−$C_2H_4O_2$−OH	BTG-14 and 15A-17
14	14	16	4	248	[HHH]−H_2O−$C_3H_6O_2$−CO−4OH	22A-15
15	10	18	7	250	[HH]−2H_2O−2CO	15A-8
16	15	14	4	258	[HHH]−6H_2O−$C_2H_4O_2$−4OH−CH_3	22A-16
17	15	16	4	260	[HHH]−5H_2O−$C_2H_4O_2$−5OH−CH_3	22A-6
18	11	18	7	262	[HHH]−2H_2O−CO−OH	15A-15
19	10	16	8	264	[HH]−H_2O−$C_2H_4O_2$	BTG-3 and 15A-18
20	10	20	8	268	[HH]−$C_2H_4O_2$ + H_2−OH	15A-12
21	16	18	4	274	[HHH]−5H_2O−$C_2H_4O_2$−5OH	22A-12
22	11	18	8	278	[HH]−2H_2O−CO	BTG-7 and 15A-5
23	12	16	8	288	[HH]−3H_2O	BTG-16
24	12	20	8	292	[HH]−H_2O−2OH	15A-9
25	11	20	9	296	[HH]−H_2O−CO	BTG-8 and 15A-3
26	13	16	8	300	[HHH]−4H_2O−$C_3H_6O_2$−CO−OH−CH_3	22A-19
27	12	18	9	306	[HH]−2H_2O	BTG-19
28	12	20	9	308	[HH]−H_2O−OH	BTG-5 and 15A-7
29	14	18	8	314	[HHH]−4H_2O−$C_3H_6O_2$−CO−OH	22A-5
30	13	22	9	322	[HHH]−2H_2O−$C_3H_6O_2$−2CO−OH	15A-20
31	12	20	10	324	[HH]−H_2O (cellobiosan)	BTG-2, 15A-4, and 22A-11
32	15	18	8	326	[HHH]−5H_2O−$C_2H_4O_2$−CO	22A-9
33	15	20	8	328	[HHH]−4H_2O−$C_2H_4O_2$−CO−OH	22A-10
34	13	22	10	338	[HHH]−2H_2O−$C_3H_6O_2$−2CO	BTG-10 and 15A-2
35	14	22	10	350	[HHH]−2H_2O−$C_2H_4O_2$−CO−OH−CH_3	BTG-22 and 15A-21
36	14	24	10	352	[HHH]−2H_2O−$C_2H_4O_2$−2CO	15A-10
37	15	24	10	364	[HHH]−2H_2O−$C_2H_4O_2$−CO−OH	BTG-21
38	14	22	11	366	[HHH]−2H_2O−$C_3H_6O_2$−CO	BTG-12 and 15A-14
39	14	24	11	368	[HHH]−H_2O−$C_3H_6O_2$−CO−OH	BTG-18 and 15A-16
40	17	24	9	372	[HHH]−4H_2O−CO−2OH	22A-20
41	16	24	10	376	[HHH]−2H_2O−$C_2H_4O_2$−2OH	BTG-23
42	15	24	11	380	[HHH]−2H_2O−$C_2H_4O_2$−CO	15A-11
43	16	24	11	392	[HHH]−2H_2O−$C_2H_4O_2$−OH	BTG-13 and 15A-23
44	16	26	11	394	[HHH]−H_2O−$C_2H_4O_2$−2OH	15A-19
45	15	26	12	398	[HHH]−H_2O−$C_2H_4O_2$−CO	15A-13
46	21	26	9	422	[HHHH]−8H_2O−3CO−OH	22A-13
47	18	26	12	434	[HHH]−3H_2O−OH	BTG-20
48	22	28	9	436	[HHHH]−7H_2O−2CO−3OH	22A-23
49	18	28	13	452	[HHH]−2H_2O−OH	BTG-17
50	18	30	15	486	[HHH]−H_2O (cellotriosan)	BTG-15 and 22A-22

[a]Sample ID: name of sample (BTG, 15A, and 22A) and rank of the relative abundance for the given peak in that sample.

3.3.2. Hemicellulose- and Lignin-Derived Structures. In addition to the results presented in Table 4, it is also possible to propose matching structures for some peaks that are hemicellulose- or lignin-derived. These results are shown in Table 5 (examples of 10 from hemicellulose and 5 from lignin). This type of alternative structure matching is possible because FT-ICR MS alone does not distinguish between isomers.[94] The same naming convention is used here as previously in Table 4. The additions are P for pentose monomer units in hemicellulose and G for guaiacyl monomer units in lignin.

Interestingly, none of the top peaks for BTG and 15A bio-oils fall within the lignin region of a van Krevelen diagram (O/C ≈ 0.2−0.5; H/C ≈ 0.8−1.3); therefore, all peaks in Table 5

https://dx.doi.org/10.1021/acs.energyfuels.0c01687
Energy Fuels 2020, 34, 8466−8481

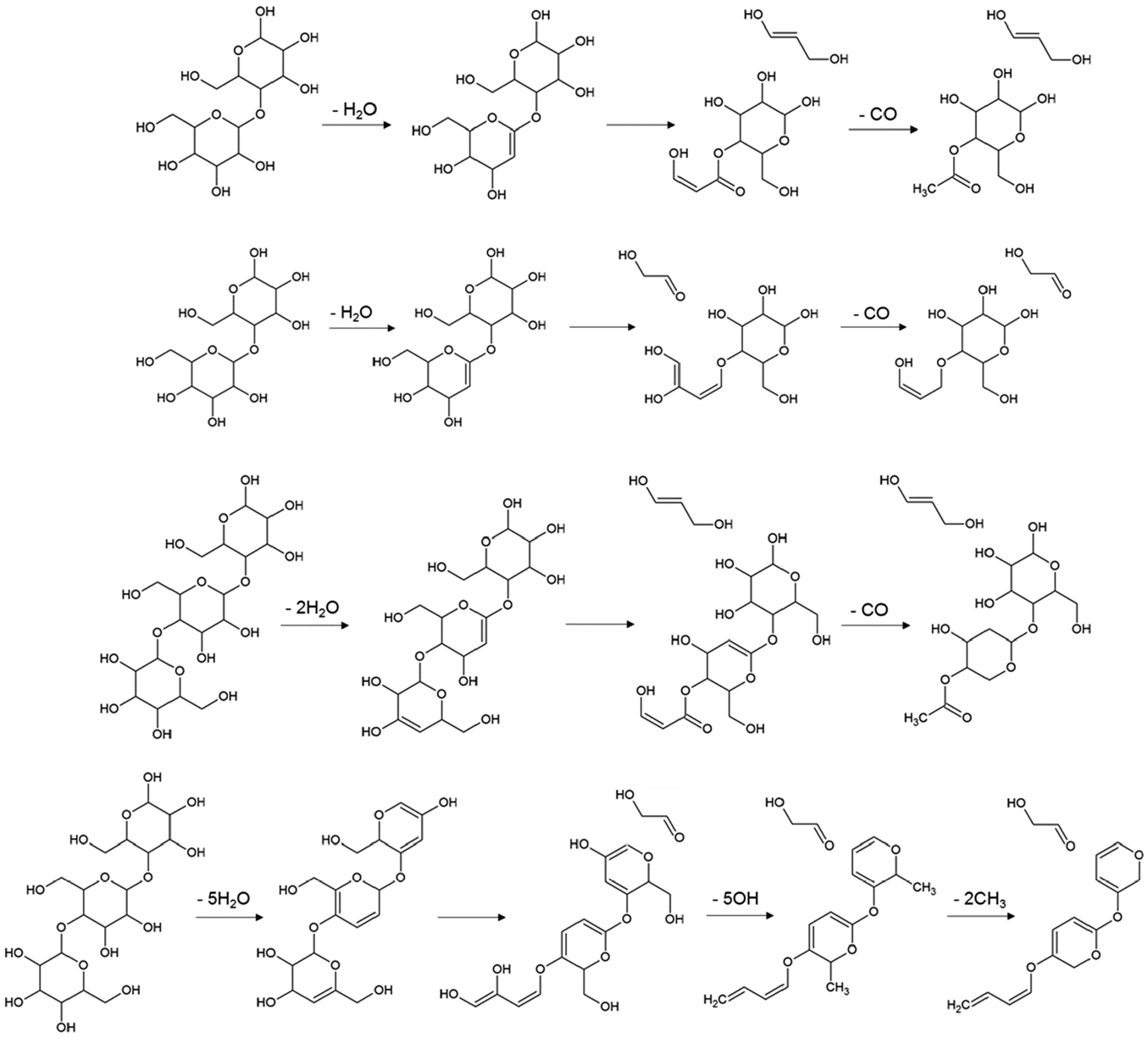

Figure 11. Hypothetical proposed pathways and final structures for oligomers reported in Table 4 (from top to bottom, numbers 8, 11, 34, and 12 in Table 4).

attributed to lignin-derived compounds are from 22A bio-oil. Additionally, it was not possible to identify top peaks in 22A that could be attributed solely to guaiacyl lignin-derived compounds alone. Because the original biomass used in pyrolysis is from pine, a softwood, syringyl and/or *p*-hydroxyphenyl-derived compounds are expected to be negligible or virtually absent.[82] The five 22A peaks that are identified result, potentially, from fragmentations of the lignin−carbohydrate complex. This lack of lignin-derived compounds among the top peaks may be the result of (1) the relative underabundance of the lignin content in biomass in comparison to holocellulose[95] and/or (2) ionization effects during ESI that favor more polar compounds. Further reading on ionization during biomass pyrolysis oil FT-ICR MS analysis is available in work from Hertzog and co-workers.[22,23,96]

3.3.3. Discussion. The presented analysis of FT-ICR MS data for biomass pyrolysis oils has significant utility for two proposed reasons. First, knowledge of molecular structure(s) allows for prediction of physical/chemical properties, thereby allowing for more efficient exploitation of those properties during valorization of the material/product. This type of work is ongoing among energy and fuel researchers and should be a point of emphasis in future studies.[31,97−100] Second, proposing routes by which fragmentations can follow to reach a desired final structure sheds light on possible mechanisms underlying biomass pyrolysis. It is shown here that the top peaks among the three samples can vary appreciably, especially with respect to the degree in which they experience fragmentation. A summary of the average O/C, H/C, and DBE/C[101] ratios for the top 23 peaks from each sample is given in Table 6. The value of these ratios for BTG and 15A are similar; however, 22A has lower O/C and H/C ratios and higher average DBE/C. These quantitative metrics indicate that the 22A sample has undergone more pyrolytic degradation than BTG and 15A samples. This is consistent with what would be expected from the effects of the particle size and temperature on pyrolysis

https://dx.doi.org/10.1021/acs.energyfuels.0c01687
Energy Fuels 2020, 34, 8466−8481

Table 5. Proposed Fragmentation Pathways and Resulting Structure Representation for Hemicellulose and Lignin Oligomer-Derived Peaks among the Studied Bio-oils

number[a]	C	H	O	mass	proposed structure	sample ID
11	9	16	7	236	[PP]−H_2O−CO (hemicellulose)	BTG-6, 15A-1, and 22A-18
13	10	16	7	248	[PH]−H_2O−OH (hemicellulose)	BTG-14 and 15A-17
15	10	18	7	250	[PP]−2OH (hemicellulose)	15A-8
18	11	18	7	262	[PH]−H_2O−OH (hemicellulose)	15A-15
19	10	16	8	264	[PP]−H_2O (hemicellulose)	BTG-3 and 15A-18
22	11	18	8	278	[PH]−H_2O (hemicellulose)	BTG-7 and 15A-5
25	11	20	9	296	[PH] (hemicellulose)	BTG-8 and 15A-3
42	15	24	11	380	[PPP]−H_2O−OH (hemicellulose)	15A-11
43	16	24	11	392	[PPH]−$2H_2O$ (hemicellulose)	BTG-13 and 15A-23
45	15	26	12	398	[PPP]−OH (hemicellulose)	15A-13
9	13	12	4	232	[HG]−$3H_2O$−2CO−CH_3−$2H_2$ (lignin)	22A-4
12	14	14	4	246	[HG]−$4H_2O$−CO−CH_3 (lignin)	22A-3
17	15	16	4	260	[HG]−$4H_2O$−CO (lignin)	22A-6
29	14	18	8	314	[HG]−$2CH_3$−OH−H_2 (lignin)	22A-5
48	22	28	9	436	[HGG]−$2CH_3$−$2H_2O$−2CO (lignin)	22A-23

[a]Numbering corresponds to identical reported peaks in Table 4.

Table 6. Quantitative Parameters for Comparison of the Fragmentation Degree among Top Bio-oil Peaks

sample	O/C[a]	H/C[a]	DBE/C[a]
BTG	0.78 (0.08)	1.65 (0.11)	0.27 (0.05)
15A	0.76 (0.07)	1.70 (0.10)	0.24 (0.04)
22A	0.53 (0.24)	1.31 (0.31)	0.43 (0.14)

[a]Averages for specified parameters with weighted standard deviations in parentheses (weighting by MS abundance).

products.[68,79,102] Surveying the extent of fragmentation of the proposed structures in Table 4 for 22A bio-oil supports this view.

Assessing the results presented in Table 4 shows that, among the 50 proposed structures, 34 are suggested to have originated from reactions (specifically, retro-Diels−Alder is used here) beyond simple dehydration and/or decarbonylation. The retro-Diels−Alder mechanism was considered here primarily based on relevant computational work from Easton et al., who suggest that this mechanism is thermodynamically favorable, with low transition state energies for reactions of water-loss products from pyrolysis of cellobiose.[81] As an illustrative example, the most abundant peak from BTG and 22A (number 8 in Table 4, $C_8H_{14}O_7$) is proposed to have originated from the retro-Diels−Alder reaction of dehydrated cellobiose, with a subsequent decarbonylation following tautomerization. This product ($C_8H_{14}O_7$) is also detected in high abundance in work from Hurt et al. and Hutchinson et al., who illustrates the formation of $C_8H_{14}O_7$ through successive retro-aldol reactions.[103,104] The two routes are complementary but arrive at different $C_8H_{14}O_7$ isomers. A possible suggested pathway to the formation of $C_8H_{14}O_7$ as well as for three other abundant MS-detected products is shown in Figure 11. Although not discussed at length in this work, ongoing research seeks to address the "isomer problem" of FT-ICR MS analysis through incorporation of software tools and more advanced separation and/or hybridized techniques.[105−110]

Taken as a whole, the proposed pathways by which FT-ICR MS-detected oligomeric structures can be derived are consistent with the overview of pyrolysis discussed by Stankovikj et al. and others.[24,66,71,72,80] Initially, cellulose (or other biomass constituent) decomposes from a singular polymer into monomers directly and/or a variety of oligomers of $d_p \approx 2-5$. These oligomers continue to undergo dehydration and fragmentation reactions to produce gases, light volatile organics, and more highly degraded pyrolytic lignins and humins. By proceeding via the pathways shown in Table 4, we have shown that pyrolytic humin structures can be reached from unmodified cellulose-derived oligomers, while at the same time producing H_2O, CO, and C_2-C_3 light volatile organics. Once primary oligomers have been sufficiently modified within a reactive liquid intermediate phase, they can be collected as GC/MS- and/or FT-ICR MS-detectable liquid products through either evaporation or thermal ejection as aerosols. A significant fraction may also continue reacting to form solid-phase char.

Specifically, one possible degraded oligomer formation pathway suggested in this work is through thermodynamically favorable retro-Diels−Alder reactions, yielding C_2-C_3 products, which are known to be abundant from pyrolysis.[24,32] It is certainly probable that other classes of reactions may also occur with equal or greater frequency. Some of these transformations (for cellulose) include retro-aldol reactions, ring opening, and/or flipping, cyclization, and tautomerization.[11] The need for differentiating among these primary mechanisms and their relevant product isomers underscores the utility of continued novel experimental work (e.g., isotopic labeling)[111−117] and computational kinetic and thermodynamic pyrolysis studies.[81,88,118−122] Finally, the coupling of rigorous experimental kinetic study with high-resolution MS can enable the development of more detailed microkinetic models for pyrolysis, furthering the understanding of the formation of oligomers. Although the results presented here are with respect to whole biomass pyrolysis oil, the novel approach should, in theory, be extensible to other feedstocks with analogous degradation chemistry and characterization (e.g., coal tar, solid waste pyrolysis, and hydrothermal liquefaction).

4. CONCLUSION

In this study, FT-ICR MS results from three contrasting bio-oils were analyzed in depth to develop a novel strategy for oligomer structure proposal/assignment. Elemental analysis using a combination of GC/MS results for monomers and FT-

https://dx.doi.org/10.1021/acs.energyfuels.0c01687
Energy Fuels 2020, 34, 8466−8481

ICR MS results for oligomers showed good agreement with reported elemental analysis from earlier work. The bio-oil samples were presented in the forms of van Krevelen and carbon number versus mass diagrams to highlight potential fragmentation pathways. Additionally, simple combinatoric fragmentation modeling was performed for hypothetical cellulose-, hemicellulose-, and lignin-derived oligomers. This library of modeled structures/formulas was compared to FT-ICR MS-detected oligomer formulas to propose hypothetical structures and their associated fragmentation pathways. In this way, we show potential routes by which these oligomers are formed. Ultimately these pathways are consistent with present perspectives on reaction mechanisms underlying biomass pyrolysis. This work supports the central hypothesis that if the formation primary biomass pyrolysis oligomers can be developed computationally, then bio-oil characteristics *in silico* should reproduce laboratory analytical chemistry data, such as for high-resolution FT-ICR MS. The presented analytical scheme for bio-oil oligomers, featuring the coupling of high-resolution MS and reaction/fragmentation modeling, offers a novel strategy to further the understanding of biomass pyrolysis reactions at the molecular level for future micro-kinetic studies.

■ ASSOCIATED CONTENT

Supporting Information

The Supporting Information is available free of charge at https://pubs.acs.org/doi/10.1021/acs.energyfuels.0c01687.

Pyrolysis reactor schematics from Venderbosch and Prins,[77] reacting biomass particle model figure from Marathe et al.,[80] and descriptive figures of the combinatorics underlying the fragmentation modeling (PDF)

■ AUTHOR INFORMATION

Corresponding Author

Manuel Garcia-Perez − *Biological Systems Engineering and Bioproducts, Sciences, & Engineering Laboratory, Washington State University, Pullman, Washington 99163, United States;* orcid.org/0000-0002-9386-2632; Phone: 509-372-7461; Email: mgarcia-perez@wsu.edu

Author

Evan Terrell − *Biological Systems Engineering, Washington State University, Pullman, Washington 99163, United States;* orcid.org/0000-0002-1079-4110

Complete contact information is available at: https://pubs.acs.org/10.1021/acs.energyfuels.0c01687

Notes

The authors declare no competing financial interest.

■ ACKNOWLEDGMENTS

The authors acknowledge the financial contributions received from the United States Department of Energy (DE-EE0008505) and the United States National Science Foundation (NSF-CBET 1926412). Manuel Garcia-Perez is also very thankful to the United States Department of Agriculture's National Institute of Food and Agriculture through the Hatch Project (WNP00701) for funding his research program.

■ REFERENCES

(1) Dhillon, R. S.; von Wuehlisch, G. Mitigation of Global Warming through Renewable Biomass. *Biomass Bioenergy* **2013**, *48*, 75−89.

(2) Ubando, A. T.; Rivera, D. R. T.; Chen, W. H.; Culaba, A. B. A Comprehensive Review of Life Cycle Assessment (LCA) of Microalgal and Lignocellulosic Bioenergy Products from Thermochemical Processes. *Bioresour. Technol.* **2019**, *291* (July), 121837.

(3) Lazarevic, D.; Martin, M. Life Cycle Assessments, Carbon Footprints and Carbon Visions: Analysing Environmental Systems Analyses of Transportation Biofuels in Sweden. *J. Cleaner Prod.* **2016**, *137*, 249−257.

(4) Alonso, D. M.; Hakim, S. H.; Zhou, S.; Won, W.; Hosseinaei, O.; Tao, J.; Garcia-Negron, V.; Motagamwala, A. H.; Mellmer, M. A.; Huang, K.; Houtman, C. J.; Labbe, N.; Harper, D. P.; Maravelias, C.; Runge, T.; Dumesic, J. A. Increasing the Revenue from Lignocellulosic Biomass: Maximizing Feedstock Utilization. *Sci. Adv.* **2017**, *3* (5), e1603301.

(5) Le Brech, Y.; Delmotte, L.; Raya, J.; Brosse, N.; Gadiou, R.; Dufour, A. High Resolution Solid State 2D NMR Analysis of Biomass and Biochar. *Anal. Chem.* **2015**, *87* (2), 843−847.

(6) Yamaguchi, A.; Mimura, N.; Shirai, M.; Sato, O. Cascade Utilization of Biomass: Strategy for Conversion of Cellulose, Hemicellulose, and Lignin into Useful Chemicals. *ACS Sustainable Chem. Eng.* **2019**, *7* (12), 10445−10451.

(7) Buendia-Kandia, F.; Brosse, N.; Petitjean, D.; Mauviel, G.; Rondags, E.; Guedon, E.; Dufour, A. Hydrothermal Conversion of Wood, Organosolv, and Chlorite Pulps. *Biomass Convers. Biorefin.* **2020**, *10* (1), 1−13.

(8) Ciesielski, P. N.; Pecha, M. B.; Lattanzi, A. M.; Bharadwaj, V. S.; Crowley, M. F.; Bu, L.; Vermaas, J. V.; Steirer, K. X.; Crowley, M. F. Advances in Multiscale Modeling of Lignocellulosic Biomass. *ACS Sustainable Chem. Eng.* **2020**, *8* (9), 3512−3531.

(9) Yoo, C. G.; Meng, X.; Pu, Y.; Ragauskas, A. J. The Critical Role of Lignin in Lignocellulosic Biomass Conversion and Recent Pretreatment Strategies: A Comprehensive Review. *Bioresour. Technol.* **2020**, *301*, 122784.

(10) Perkins, G.; Bhaskar, T.; Konarova, M. Process Development Status of Fast Pyrolysis Technologies for the Manufacture of Renewable Transport Fuels from Biomass. *Renewable Sustainable Energy Rev.* **2018**, *90* (March), 292−315.

(11) Vinu, R.; Broadbelt, L. J. A Mechanistic Model of Fast Pyrolysis of Glucose-Based Carbohydrates to Predict Bio-oil Composition. *Energy Environ. Sci.* **2012**, *5* (12), 9808−9826.

(12) Zhou, X.; Li, W.; Mabon, R.; Broadbelt, L. J. A Mechanistic Model of Fast Pyrolysis of Hemicellulose. *Energy Environ. Sci.* **2018**, *11* (5), 1240−1260.

(13) Yanez, A. J.; Natarajan, P.; Li, W.; Mabon, R.; Broadbelt, L. J. Coupled Structural and Kinetic Model of Lignin Fast Pyrolysis. *Energy Fuels* **2018**, *32* (2), 1822−1830.

(14) Pecha, M. B.; Arbelaez, J. I. M.; Garcia-Perez, M.; Chejne, F.; Ciesielski, P. N. Progress in Understanding the Four Dominant Intra-Particle Phenomena of Lignocellulose Pyrolysis: Chemical Reactions, Heat Transfer, Mass Transfer, and Phase Change. *Green Chem.* **2019**, *21* (11), 2868−2898.

(15) Ciesielski, P. N.; Pecha, M. B.; Bharadwaj, V. S.; Mukarakate, C.; Leong, G. J.; Kappes, B.; Crowley, M. F.; Kim, S.; Foust, T. D.; Nimlos, M. R. Advancing Catalytic Fast Pyrolysis through Integrated Multiscale Modeling and Experimentation: Challenges, Progress, and Perspectives. *Wiley Interdiscip. Rev. Energy Environ.* **2018**, *7* (4), e297.

(16) Aubriet, F.; Ghislain, T.; Hertzog, J.; Sonnette, A.; Dufour, A.; Mauviel, G.; Carré, V. Characterization of Biomass and Biochar by LDI-FTICRMS—Effect of the Laser Wavelength and Biomass Material. *J. Am. Soc. Mass Spectrom.* **2018**, *29* (10), 1951−1962.

(17) Lehto, J.; Oasmaa, A.; Solantausta, Y.; Kytö, M.; Chiaramonti, D. Review of Fuel Oil Quality and Combustion of Fast Pyrolysis Bio-oils from Lignocellulosic Biomass. *Appl. Energy* **2014**, *116*, 178−190.

(18) Oasmaa, A.; Källi, A.; Lindfors, C.; Elliott, D. C.; Springer, D.; Peacocke, C.; Chiaramonti, D. Guidelines for Transportation,

Handling, and Use of Fast Pyrolysis Bio-oil. 1. Flammability and Toxicity. *Energy Fuels* **2012**, *26* (6), 3864−3873.
(19) Oasmaa, A.; Fonts, I.; Pelaez-Samaniego, M. R.; Garcia-Perez, M. E.; Garcia-Perez, M. Pyrolysis Oil Multiphase Behavior and Phase Stability: A Review. *Energy Fuels* **2016**, *30* (8), 6179−6200.
(20) Wang, Y.; Han, Y.; Hu, W.; Fu, D.; Wang, G. Analytical Strategies for Chemical Characterization of Bio-oil. *J. Sep. Sci.* **2020**, *43* (1), 360−371.
(21) Michailof, C. M.; Kalogiannis, K. G.; Sfetsas, T.; Patiaka, D. T.; Lappas, A. A. Advanced Analytical Techniques for Bio-oil Characterization. *Wiley Interdiscip. Rev. Energy Environ.* **2016**, *5* (6), 614−639.
(22) Hertzog, J.; Carré, V.; Le Brech, Y.; Dufour, A.; Aubriet, F. Toward Controlled Ionization Conditions for ESI-FT-ICR-MS Analysis of Bio-oils from Lignocellulosic Material. *Energy Fuels* **2016**, *30* (7), 5729−5739.
(23) Hertzog, J.; Carré, V.; Le Brech, Y.; Mackay, C. L.; Dufour, A.; Mašek, O.; Aubriet, F. Combination of Electrospray Ionization, Atmospheric Pressure Photoionization and Laser Desorption Ionization Fourier Transform Ion Cyclotronic Resonance Mass Spectrometry for the Investigation of Complex Mixtures—Application to the Petroleomic Analysis. *Anal. Chim. Acta* **2017**, *969*, 26−34.
(24) Stankovikj, F.; McDonald, A. G.; Helms, G. L.; Garcia-Perez, M. Quantification of Bio-oil Functional Groups and Evidences of the Presence of Pyrolytic Humins. *Energy Fuels* **2016**, *30* (8), 6505−6524.
(25) Stankovikj, F.; Garcia-Perez, M. TG-FTIR Method for the Characterization of Bio-oils in Chemical Families. *Energy Fuels* **2017**, *31* (2), 1689−1701.
(26) Stankovikj, F.; McDonald, A. G.; Helms, G. L.; Olarte, M. V.; Garcia-Perez, M. Characterization of the Water-Soluble Fraction of Woody Biomass Pyrolysis Oils. *Energy Fuels* **2017**, *31* (2), 1650−1664.
(27) Ruiz, M.; Valette, J.; Broust, F.; Bonfils, F. Rapid Quantification and Characterization of the Pyrolytic Lignin Fraction of Bio-oils by Size Exclusion Chromatography Coupled with Multi-Angle Laser Light Scattering Detector (SEC-MALS). *J. Anal. Appl. Pyrolysis* **2019**, *142* (March), 104662.
(28) Sharifzadeh, M.; Sadeqzadeh, M.; Guo, M.; Borhani, T. N.; Murthy Konda, N. V. S. N.; Garcia, M. C.; Wang, L.; Hallett, J.; Shah, N. The Multi-Scale Challenges of Biomass Fast Pyrolysis and Bio-oil Upgrading: Review of the State of Art and Future Research Directions. *Prog. Energy Combust. Sci.* **2019**, *71*, 1−80.
(29) Chu, S.; Majumdar, A. Opportunities and Challenges for a Sustainable Energy Future. *Nature* **2012**, *488* (7411), 294−303.
(30) Hansen, S.; Mirkouei, A.; Diaz, L. A. A Comprehensive State-of-Technology Review for Upgrading Bio-oil to Renewable or Blended Hydrocarbon Fuels. *Renewable Sustainable Energy Rev.* **2020**, *118*, 109548.
(31) Terrell, E.; Dellon, L. D.; Dufour, A.; Bartolomei, E.; Broadbelt, L. J.; Garcia-Perez, M. A Review on Lignin Liquefaction: Advanced Characterization of Structure and Microkinetic Modeling. *Ind. Eng. Chem. Res.* **2020**, *59* (2), 526−555.
(32) Pinheiro Pires, A. P.; Arauzo, J.; Fonts, I.; Domine, M. E.; Fernández Arroyo, A.; Garcia-Perez, M. E.; Montoya, J.; Chejne, F.; Pfromm, P.; Garcia-Perez, M. Challenges and Opportunities for Bio-oil Refining: A Review. *Energy Fuels* **2019**, *33* (6), 4683−4720.
(33) Harman-Ware, A. E.; Ferrell, J. R., III Methods and Challenges in the Determination of Molecular Weight Metrics of Bio-oils. *Energy Fuels* **2018**, *32* (9), 8905−8920.
(34) Bayerbach, R.; Meier, D. Characterization of the Water-Insoluble Fraction from Fast Pyrolysis Liquids (Pyrolytic Lignin). Part IV: Structure Elucidation of Oligomeric Molecules. *J. Anal. Appl. Pyrolysis* **2009**, *85* (1−2), 98−107.
(35) Van Zandvoort, I.; Wang, Y.; Rasrendra, C. B.; Van Eck, E. R. H.; Bruijnincx, P. C. A.; Heeres, H. J.; Weckhuysen, B. M. Formation, Molecular Structure, and Morphology of Humins in Biomass Conversion: Influence of Feedstock and Processing Conditions. *ChemSusChem* **2013**, *6* (9), 1745−1758.
(36) Comisarow, M. B.; Marshall, A. G. Fourier Transform Ion Cyclotron Resonance Spectroscopy. *Chem. Phys. Lett.* **1974**, *25* (2), 282−283.
(37) Marshall, A. G.; Grosshans, P. B. Fourier Transform Ion Cyclotron Resonance Mass Spectrometry: The Teenage Years. *Anal. Chem.* **1991**, *63* (4), 215A−229A.
(38) Marshall, A. G.; Hendrickson, C. L.; Jackson, G. S. Fourier Transform Ion Cyclotron Resonance Mass Spectrometry: A Primer. *Mass Spectrom. Rev.* **1998**, *17*, 1−35.
(39) Marshall, A. G. Fourier Transform Ion Cyclotron Resonance Mass Spectrometry. *Acc. Chem. Res.* **1985**, *18* (10), 316−322.
(40) Niyonsaba, E.; Manheim, J. M.; Yerabolu, R.; Kenttämaa, H. I. Recent Advances in Petroleum Analysis by Mass Spectrometry. *Anal. Chem.* **2019**, *91* (1), 156−177.
(41) Marshall, A. G.; Rodgers, R. P. Petroleomics: Chemistry of the Underworld. *Proc. Natl. Acad. Sci. U. S. A.* **2008**, *105* (47), 18090−18095.
(42) Chacón-Patiño, M. L.; Rowland, S. M.; Rodgers, R. P. Advances in Asphaltene Petroleomics. Part 1: Asphaltenes Are Composed of Abundant Island and Archipelago Structural Motifs. *Energy Fuels* **2017**, *31* (12), 13509−13518.
(43) Chacón-Patiño, M. L.; Rowland, S. M.; Rodgers, R. P. Advances in Asphaltene Petroleomics. Part 2: Selective Separation Method That Reveals Fractions Enriched in Island and Archipelago Structural Motifs by Mass Spectrometry. *Energy Fuels* **2018**, *32* (1), 314−328.
(44) Chacón-Patiño, M. L.; Rowland, S. M.; Rodgers, R. P. Advances in Asphaltene Petroleomics. Part 3. Dominance of Island or Archipelago Structural Motif Is Sample Dependent. *Energy Fuels* **2018**, *32* (9), 9106−9120.
(45) Nebbioso, A.; Piccolo, A. Molecular Characterization of Dissolved Organic Matter (DOM): A Critical Review. *Anal. Bioanal. Chem.* **2013**, *405* (1), 109−124.
(46) Blackburn, J. W. T.; Kew, W.; Graham, M. C.; Uhrín, D. Laser Desorption/Ionization Coupled to FTICR Mass Spectrometry for Studies of Natural Organic Matter. *Anal. Chem.* **2017**, *89* (8), 4382−4386.
(47) Zark, M.; Dittmar, T. Universal Molecular Structures in Natural Dissolved Organic Matter. *Nat. Commun.* **2018**, *9* (1), 1−8.
(48) Mopper, K.; Stubbins, A.; Ritchie, J. D.; Bialk, H. M.; Hatcher, P. G. Advanced Instrumental Approaches for Characterization of Marine Dissolved Organic Matter: Extraction Techniques, Mass Spectrometry, and Nuclear Magnetic Resonance Spectroscopy. *Chem. Rev.* **2007**, *107* (2), 419−442.
(49) Holguin, F. O.; Schaub, T. Characterization of Microalgal Lipid Feedstock by Direct-Infusion FT-ICR Mass Spectrometry. *Algal Res.* **2013**, *2* (1), 43−50.
(50) Kuhnert, N. Unraveling the Structure of the Black Tea Thearubigins. *Arch. Biochem. Biophys.* **2010**, *501* (1), 37−51.
(51) Rockenbach, I. I.; Jungfer, E.; Ritter, C.; Santiago-Schübel, B.; Thiele, B.; Fett, R.; Galensa, R. Characterization of Flavan-3-Ols in Seeds of Grape Pomace by CE, HPLC-DAD-MS n and LC-ESI-FTICR-MS. *Food Res. Int.* **2012**, *48* (2), 848−855.
(52) Shrestha, B.; le Brech, Y.; Ghislain, T.; Leclerc, S.; Carré, V.; Aubriet, F.; Hoppe, S.; Marchal, P.; Pontvianne, S.; Brosse, N.; Dufour, A. A Multitechnique Characterization of Lignin Softening and Pyrolysis. *ACS Sustainable Chem. Eng.* **2017**, *5* (8), 6940−6949.
(53) Garcia-Pérez, M.; Terrell, E.; Carré, V.; Doufour, A.; Aubriet, F.; Le Brech, Y. Contributions to Lignomics: Stochastic Generation of Oligomeric Lignin Structures for Interpretation of MALDI−FT-ICR-MS Results. *ChemSusChem* **2020**, DOI: 10.1002/cssc.202000239.
(54) Xiong, Z.; Guo, J.; Chaiwat, W.; Deng, W.; Hu, X.; Han, H.; Chen, Y.; Xu, K.; Su, S.; Hu, S.; Wang, Y.; Xiang, J. Assessing the Chemical Composition of Heavy Components in Bio-oils from the Pyrolysis of Cellulose, Hemicellulose and Lignin at Slow and Fast Heating Rates. *Fuel Process. Technol.* **2020**, *199*, 106299.
(55) McClelland, D. J.; Motagamwala, A. H.; Li, Y.; Rover, M. R.; Wittrig, A. M.; Wu, C.; Buchanan, J. S.; Brown, R. C.; Ralph, J.; Dumesic, J. A.; Huber, G. W. Functionality and Molecular Weight

https://dx.doi.org/10.1021/acs.energyfuels.0c01687
Energy Fuels 2020, 34, 8466−8481

Distribution of Red Oak Lignin before and after Pyrolysis and Hydrogenation. *Green Chem.* **2017**, *19* (5), 1378−1389.
(56) Yan, H.-L.; Li, Z.-K.; Wang, Z.-C.; Lei, Z.-P.; Ren, S.-B.; Pan, C.-X.; Tian, Y.-J.; Kang, S.-G.; Yan, J.-C.; Shui, H.-F. Characterization of Soluble Portions from Cellulose, Hemicellulose, and Lignin Methanolysis. *Fuel* **2019**, *246*, 394−401.
(57) Jarvis, J. M.; Billing, J. M.; Corilo, Y. E.; Schmidt, A. J.; Hallen, R. T.; Schaub, T. M. FT-ICR MS Analysis of Blended Pine-Microalgae Feedstock HTL Biocrudes. *Fuel* **2018**, *216*, 341−348.
(58) Palacio Lozano, D. C.; Ramírez, C. X.; Sarmiento Chaparro, J. A.; Thomas, M. J.; Gavard, R.; Jones, H. E.; Cabanzo Hernández, R.; Mejia-Ospino, E.; Barrow, M. P. Characterization of Bio-Crude Components Derived from Pyrolysis of Soft Wood and Its Esterified Product by Ultrahigh Resolution Mass Spectrometry and Spectroscopic Techniques. *Fuel* **2020**, *259*, 116085.
(59) Leonardis, I.; Chiaberge, S.; Fiorani, T.; Spera, S.; Battistel, E.; Bosetti, A.; Cesti, P.; Reale, S.; De Angelis, F. Characterization of Bio-oil from Hydrothermal Liquefaction of Organic Waste by NMR Spectroscopy and FTICR Mass Spectrometry. *ChemSusChem* **2013**, *6* (1), 160−167.
(60) Olcese, R.; Carré, V.; Aubriet, F.; Dufour, A. Selectivity of Bio-oils Catalytic Hydrotreatment Assessed by Petroleomic and GC*GC/MS-FID Analysis. *Energy Fuels* **2013**, *27* (4), 2135−2145.
(61) Ware, R. L.; Rodgers, R. P.; Marshall, A. G.; Mante, O. D.; Dayton, D. C.; Verdier, S.; Gabrielsen, J.; Rowland, S. M. Detailed Chemical Composition of an Oak Biocrude and Its Hydrotreated Product Determined by Positive Atmospheric Pressure Photoionization Fourier Transform Ion Cyclotron Resonance Mass Spectrometry. *Sustain. Energy Fuels* **2020**, *4*, 2404−2410.
(62) Dellon, L. D.; Yanez, A. J.; Li, W.; Mabon, R.; Broadbelt, L. J. Computational Generation of Lignin Libraries from Diverse Biomass Sources. *Energy Fuels* **2017**, *31* (8), 8263−8274.
(63) Yanez, A. J.; Li, W.; Mabon, R.; Broadbelt, L. J. A Stochastic Method to Generate Libraries of Structural Representations of Lignin. *Energy Fuels* **2016**, *30* (7), 5835−5845.
(64) Orella, M. J.; Gani, T. Z. H.; Vermaas, J. V.; Stone, M. L.; Anderson, E. M.; Beckham, G. T.; Brushett, F. R.; Román-Leshkov, Y. Lignin-KMC: A Toolkit for Simulating Lignin Biosynthesis. *ACS Sustainable Chem. Eng.* **2019**, *7*, 18313−18322.
(65) Zhou, X.; Li, W.; Mabon, R.; Broadbelt, L. J. A Critical Review on Hemicellulose Pyrolysis. *Energy Technol.* **2017**, *5* (1), 52−79.
(66) Marathe, P. S.; Westerhof, R. J. M.; Kersten, S. R. A. Fast Pyrolysis of Lignins with Different Molecular Weight: Experiments and Modelling. *Appl. Energy* **2019**, *236*, 1125−1137.
(67) Collard, F. X.; Blin, J. A Review on Pyrolysis of Biomass Constituents: Mechanisms and Composition of the Products Obtained from the Conversion of Cellulose, Hemicelluloses and Lignin. *Renewable Sustainable Energy Rev.* **2014**, *38*, 594−608.
(68) Ansari, K. B.; Arora, J. S.; Chew, J. W.; Dauenhauer, P. J.; Mushrif, S. H. Fast Pyrolysis of Cellulose, Hemicellulose, and Lignin: Effect of Operating Temperature on Bio-oil Yield and Composition and Insights into the Intrinsic Pyrolysis Chemistry. *Ind. Eng. Chem. Res.* **2019**, *58* (35), 15838−15852.
(69) Anca-Couce, A. Reaction Mechanisms and Multi-Scale Modelling of Lignocellulosic Biomass Pyrolysis. *Prog. Energy Combust. Sci.* **2016**, *53* (2016), 41−79.
(70) Kan, T.; Strezov, V.; Evans, T. J. Lignocellulosic Biomass Pyrolysis: A Review of Product Properties and Effects of Pyrolysis Parameters. *Renewable Sustainable Energy Rev.* **2016**, *57*, 1126−1140.
(71) Pecha, M. B.; Terrell, E.; Montoya, J. I.; Stankovikj, F.; Broadbelt, L. J.; Chejne, F.; Garcia-Perez, M. Effect of Pressure on Pyrolysis of Milled Wood Lignin and Acid-Washed Hybrid Poplar Wood. *Ind. Eng. Chem. Res.* **2017**, *56* (32), 9079−9089.
(72) Pecha, M. B.; Montoya, J. I.; Chejne, F.; Garcia-Perez, M. Effect of a Vacuum on the Fast Pyrolysis of Cellulose: Nature of Secondary Reactions in a Liquid Intermediate. *Ind. Eng. Chem. Res.* **2017**, *56* (15), 4288−4301.
(73) Retzekas, E.; Voutsas, E.; Magoulas, K.; Tassios, D. Prediction of Physical Properties of Hydrocarbons, Petroleum, and Coal Liquid Fractions. *Ind. Eng. Chem. Res.* **2002**, *41* (6), 1695−1702.
(74) Stein, S. E.; Brown, R. L. Estimation of Normal Boiling Points from Group Contributions. *J. Chem. Inf. Model.* **1994**, *34* (3), 581−587.
(75) Stefanis, E.; Constantinou, L.; Panayiotou, C. A Group-Contribution Method for Predicting Pure Component Properties of Biochemical and Safety Interest. *Ind. Eng. Chem. Res.* **2004**, *43* (19), 6253−6261.
(76) Just, S.; Sievert, F.; Thommes, M.; Breitkreutz, J. Improved Group Contribution Parameter Set for the Application of Solubility Parameters to Melt Extrusion. *Eur. J. Pharm. Biopharm.* **2013**, *85* (3, Part B), 1191−1199.
(77) Venderbosch, R.; Prins, W. Fast Pyrolysis Technology Development. *Biofuels, Bioprod. Biorefin.* **2010**, *4* (2), 178−208.
(78) Westerhof, R. J. M. Refining Fast Pyrolysis of Biomass. Ph.D. Thesis, University of Twente, Enschede, Netherlands, 2011.
(79) Zhou, S.; Garcia-Perez, M.; Pecha, B.; Kersten, S. R. A.; McDonald, A. G.; Westerhof, R. J. M. Effect of the Fast Pyrolysis Temperature on the Primary and Secondary Products of Lignin. *Energy Fuels* **2013**, *27* (10), 5867−5877.
(80) Marathe, P. S.; Westerhof, R. J. M.; Kersten, S. R. A. Effect of Pressure and Hot Vapor Residence Time on the Fast Pyrolysis of Biomass: Experiments and Modeling. *Energy Fuels* **2020**, *34* (2), 1773−1780.
(81) Easton, M. W.; Nash, J. J.; Kenttämaa, H. I. Dehydration Pathways for Glucose and Cellobiose during Fast Pyrolysis. *J. Phys. Chem. A* **2018**, *122* (41), 8071−8085.
(82) Obst, J. R.; Laaducci, L. L. The Syringyl Content of Softwood Lignin. *J. Wood Chem. Technol.* **1986**, *6* (3), 311−327.
(83) Ware, R. L.; Rowland, S. M.; Rodgers, R. P.; Marshall, A. G. Advanced Chemical Characterization of Pyrolysis Oils from Landfill Waste, Recycled Plastics, and Forestry Residue. *Energy Fuels* **2017**, *31* (8), 8210−8216.
(84) Kim, S.; Kramer, R. W.; Hatcher, P. G. Graphical Method for Analysis of Ultrahigh-Resolution Broadband Mass Spectra of Natural Organic Matter, the Van Krevelen Diagram. *Anal. Chem.* **2003**, *75* (20), 5336−5344.
(85) Wu, Z.; Rodgers, R. P.; Marshall, A. G. Two- and Three-Dimensional van Krevelen Diagrams: A Graphical Analysis Complementary to the Kendrick Mass Plot for Sorting Elemental Compositions of Complex Organic Mixtures Based on Ultrahigh-Resolution Broadband Fourier Transform Ion Cyclotron Resonance. *Anal. Chem.* **2004**, *76* (9), 2511−2516.
(86) Reemtsma, T. The Carbon versus Mass Diagram to Visualize and Exploit FTICR-MS Data of Natural Organic Matter. *J. Mass Spectrom.* **2010**, *45* (4), 382−390.
(87) Tang, M. M.; Bacon, R. Carbonization of Cellulose Fibers-I. Low Temperature Pyrolysis. *Carbon* **1964**, *2* (3), 211−220.
(88) Mayes, H. B.; Broadbelt, L. J. Unraveling the Reactions That Unravel Cellulose. *J. Phys. Chem. A* **2012**, *116* (26), 7098−7106.
(89) Zhang, Y.; Liu, C.; Xie, H. Mechanism Studies on β-D-Glucopyranose Pyrolysis by Density Functional Theory Methods. *J. Anal. Appl. Pyrolysis* **2014**, *105*, 23−34.
(90) Patwardhan, P. R.; Satrio, J. A.; Brown, R. C.; Shanks, B. H. Product Distribution from Fast Pyrolysis of Glucose-Based Carbohydrates. *J. Anal. Appl. Pyrolysis* **2009**, *86* (2), 323−330.
(91) Patwardhan, P. R.; Brown, R. C.; Shanks, B. H. Product Distribution from the Fast Pyrolysis of Hemicellulose. *ChemSusChem* **2011**, *4* (5), 636−643.
(92) Klein, M. T.; Virk, P. S. Modeling of Lignin Thermolysis. *Energy Fuels* **2008**, *22* (4), 2175−2182.
(93) Patwardhan, P. R.; Brown, R. C.; Shanks, B. H. Understanding the Fast Pyrolysis of Lignin. *ChemSusChem* **2011**, *4* (11), 1629−1636.
(94) Hertkorn, N.; Frommberger, M.; Witt, M.; Koch, B. P.; Schmitt-Kopplin, P.; Perdue, E. M. Natural Organic Matter and the Event Horizon of Mass Spectrometry. *Anal. Chem.* **2008**, *80* (23), 8908−8919.

https://dx.doi.org/10.1021/acs.energyfuels.0c01687
Energy Fuels 2020, 34, 8466−8481

(95) Vassilev, S. V.; Baxter, D.; Andersen, L. K.; Vassileva, C. G.; Morgan, T. J. An Overview of the Organic and Inorganic Phase Composition of Biomass. *Fuel* **2012**, *94*, 1−33.
(96) Hertzog, J.; Carré, V.; Dufour, A.; Aubriet, F. Semi-Targeted Analysis of Complex Matrices by ESI FT-ICR MS or How an Experimental Bias May Be Used as an Analytical Tool. *J. Am. Soc. Mass Spectrom.* **2018**, *29* (3), 543−557.
(97) Li, R.; Herreros, J. M.; Tsolakis, A.; Yang, W. Novel Functional Group Contribution Method for Surrogate Formulation with Accurate Fuel Compositions. *Energy Fuels* **2020**, *34* (3), 2989−3012.
(98) Ganesh, H. S.; Dean, D. P.; Vernuccio, S.; Edgar, T. F.; Baldea, M.; Broadbelt, L. J.; Stadtherr, M. A.; Allen, D. T. Product Value Modeling for a Natural Gas Liquid to Liquid Transportation Fuel Process. *Ind. Eng. Chem. Res.* **2020**, *59* (7), 3109−3119.
(99) Florido, P. M.; Visioli, P. C. F.; Pinto, C. N.; Gonçalves, C. B. Study of FAME Model Systems: Database and Evaluation of Predicting Models for Biodiesel Physical Properties. *Renewable Energy* **2020**, *151*, 837−845.
(100) Prieto, M. G.; Sánchez, F. A.; Pereda, S. Modeling Phase Equilibria of Ethers and Alcohols with GCA-EOS for Assessing the Coblending of Advanced Biofuels. *J. Chem. Eng. Data* **2019**, *64* (6), 2504−2518.
(101) Hockaday, W. C.; Grannas, A. M.; Kim, S.; Hatcher, P. G. Direct Molecular Evidence for the Degradation and Mobility of Black Carbon in Soils from Ultrahigh-Resolution Mass Spectral Analysis of Dissolved Organic Matter from a Fire-Impacted Forest Soil. *Org. Geochem.* **2006**, *37* (4), 501−510.
(102) Garcia-Perez, M.; Wang, X. S.; Shen, J.; Rhodes, M. J.; Tian, F.; Lee, W. J.; Wu, H.; Li, C. Z. Fast Pyrolysis of Oil Mallee Woody Biomass: Effect of Temperature on the Yield and Quality of Pyrolysis Products. *Ind. Eng. Chem. Res.* **2008**, *47* (6), 1846−1854.
(103) Hurt, M. R.; Degenstein, J. C.; Gawecki, P.; Borton, D. J.; Vinueza, N. R.; Yang, L.; Agrawal, R.; Delgass, W. N.; Ribeiro, F. H.; Kenttämaa, H. I. On-Line Mass Spectrometric Methods for the Determination of the Primary Products of Fast Pyrolysis of Carbohydrates and for Their Gas-Phase Manipulation. *Anal. Chem.* **2013**, *85* (22), 10927−10934.
(104) Hutchinson, C. P.; Cole, D. P.; Dalluge, E. A.; Larson, E. A.; Lee, Y. J. Novel Instrumentation for Tracking Molecular Products in Fast Pyrolysis of Carbohydrates with Sub-Second Temporal Resolution. *J. Anal. Appl. Pyrolysis* **2018**, *136*, 107−114.
(105) Lu, K.; Gardner, W. S.; Liu, Z. Molecular Structure Characterization of Riverine and Coastal Dissolved Organic Matter with Ion Mobility Quadrupole Time-of-Flight LCMS (IM Q-TOF LCMS). *Environ. Sci. Technol.* **2018**, *52* (13), 7182−7191.
(106) Owen, B. C.; Haupert, L. J.; Jarrell, T. M.; Marcum, C. L.; Parsell, T. H.; Abu-Omar, M. M.; Bozell, J. J.; Black, S. K.; Kenttämaa, H. I. High-Performance Liquid Chromatography/High-Resolution Multiple Stage Tandem Mass Spectrometry Using Negative-Ion-Mode Hydroxide-Doped Electrospray Ionization for the Characterization of Lignin Degradation Products. *Anal. Chem.* **2012**, *84* (14), 6000−6007.
(107) Reymond, C.; Dubuis, A.; Le Masle, A.; Colas, C.; Chahen, L.; Destandau, E.; Charon, N. Characterization of Liquid−Liquid Extraction Fractions from Lignocellulosic Biomass by High Performance Liquid Chromatography Hyphenated to Tandem High-Resolution Mass Spectrometry. *J. Chromatogr. A* **2020**, *1610*, 460569.
(108) Leyva, D.; Tose, L. V.; Porter, J.; Wolff, J.; Jaffé, R.; Fernandez-Lima, F. Understanding the Structural Complexity of Dissolved Organic Matter: Isomeric Diversity. *Faraday Discuss.* **2019**, *218*, 431−440.
(109) Gavard, R.; Jones, H. E.; Palacio Lozano, D. C.; Thomas, M. J.; Rossell, D.; Spencer, S. E. F.; Barrow, M. P. KairosMS: A New Solution for the Processing of Hyphenated Ultrahigh Resolution Mass Spectrometry Data. *Anal. Chem.* **2020**, *92* (5), 3775−3786.
(110) Dubuis, A.; Le Masle, A.; Chahen, L.; Destandau, E.; Charon, N. Off-Line Comprehensive Size Exclusion Chromatography × reversed-Phase Liquid Chromatography Coupled to High Resolution Mass Spectrometry for the Analysis of Lignocellulosic Biomass Products. *J. Chromatogr. A* **2020**, *1609*, 460505.
(111) Ponder, G. R.; Richards, G. N. Pyrolysis of Some ^{13}C-Labeled Glucans: A Mechanistic Study. *Carbohydr. Res.* **1993**, *244* (1), 27−47.
(112) Paine, J. B.; Pithawalla, Y. B.; Naworal, J. D.; Thomas, C. E. Carbohydrate Pyrolysis Mechanisms from Isotopic Labeling. Part 1: The Pyrolysis of Glycerin: Discovery of Competing Fragmentation Mechanisms Affording Acetaldehyde and Formaldehyde and the Implications for Carbohydrate Pyrolysis. *J. Anal. Appl. Pyrolysis* **2007**, *80* (2), 297−311.
(113) Paine, J. B.; Pithawalla, Y. B.; Naworal, J. D. Carbohydrate Pyrolysis Mechanisms from Isotopic Labeling. Part 4. The Pyrolysis of D-Glucose: The Formation of Furans. *J. Anal. Appl. Pyrolysis* **2008**, *83* (1), 37−63.
(114) Paine, J. B.; Pithawalla, Y. B.; Naworal, J. D. Carbohydrate Pyrolysis Mechanisms from Isotopic Labeling. Part 3. The Pyrolysis of D-Glucose: Formation of C3 and C4 Carbonyl Compounds and a Cyclopentenedione Isomer by Electrocyclic Fragmentation Mechanisms. *J. Anal. Appl. Pyrolysis* **2008**, *82* (1), 42−69.
(115) Paine, J. B.; Pithawalla, Y. B.; Naworal, J. D. Carbohydrate Pyrolysis Mechanisms from Isotopic Labeling. Part 2. The Pyrolysis of D-Glucose: General Disconnective Analysis and the Formation of C1 and C2 Carbonyl Compounds by Electrocyclic Fragmentation Mechanisms. *J. Anal. Appl. Pyrolysis* **2008**, *82* (1), 10−41.
(116) Paine, J. B.; Pithawalla, Y. B.; Naworal, J. D. Carbohydrate Pyrolysis Mechanisms from Isotopic Labeling. Part 5. The Pyrolysis of D-Glucose: The Origin of the Light Gases from the D-Glucose Molecule. *J. Anal. Appl. Pyrolysis* **2019**, *138*, 70−93.
(117) Degenstein, J. C.; Murria, P.; Easton, M.; Sheng, H.; Hurt, M.; Dow, A. R.; Gao, J.; Nash, J. J.; Agrawal, R.; Delgass, W. N.; Ribeiro, F. H.; Kenttamaa, H. I. Fast Pyrolysis of ^{13}C-Labeled Cellobioses: Gaining Insights into the Mechanisms of Fast Pyrolysis of Carbohydrates. *J. Org. Chem.* **2015**, *80* (3), 1909−1914.
(118) Mayes, H. B.; Nolte, M. W.; Beckham, G. T.; Shanks, B. H.; Broadbelt, L. J. The Alpha-Bet(a) of Glucose Pyrolysis: Computational and Experimental Investigations of 5-Hydroxymethylfurfural and Levoglucosan Formation Reveal Implications for Cellulose Pyrolysis. *ACS Sustainable Chem. Eng.* **2014**, *2* (6), 1461−1473.
(119) Yang, X.; Fu, Z.; Han, D.; Zhao, Y.; Li, R.; Wu, Y. Unveiling the Pyrolysis Mechanisms of Cellulose: Experimental and Theoretical Studies. *Renewable Energy* **2020**, *147*, 1120−1130.
(120) Asatryan, R.; Bennadji, H.; Bozzelli, J. W.; Ruckenstein, E.; Khachatryan, L. Molecular Products and Fundamentally Based Reaction Pathways in the Gas-Phase Pyrolysis of the Lignin Model Compound p-Coumaryl Alcohol. *J. Phys. Chem. A* **2017**, *121* (18), 3352−3371.
(121) Asatryan, R.; Hudzik, J. M.; Bozzelli, J. W.; Khachatryan, L.; Ruckenstein, E. OH-Initiated Reactions of p-Coumaryl Alcohol Relevant to the Lignin Pyrolysis. Part I. Potential Energy Surface Analysis. *J. Phys. Chem. A* **2019**, *123* (13), 2570−2585.
(122) Kostetskyy, P.; Coile, M. W.; Terrian, J. M.; Collins, J. W.; Martin, K. J.; Brazdil, J. F.; Broadbelt, L. J. Selective Production of Glycoaldehyde via Hydrothermal Pyrolysis of Glucose: Experiments and Microkinetic Modeling. *J. Anal. Appl. Pyrolysis* **2020**, *149*, 104846.

https://dx.doi.org/10.1021/acs.energyfuels.0c01687
Energy Fuels 2020, 34, 8466−8481